SUPPLEMENT 1

HONG KONG MEDICAL JOURNAL 香港醫學雜誌 30(S1)

Volume 30 Number 1 **February 2024**

HONG KONG MEDICAL JOURNAL 香港醫學雜誌

The official publication of the
Hong Kong Academy of Medicine and
the Hong Kong Medical Association

Health and Medical Research Fund

Research Dissemination Reports

醫療衞生研究基金

研究成果報告

Infectious diseases
傳染病

Health services research
醫療服務研究

Cancer
癌症

Gastrointestinal disease
胃腸道疾病

Visual system
視覺系統

Reproductive health
生殖健康

Volume 30 Number 1 **February 2024**

Supplement 1

ISSN 1024-2708

香港醫學專科學院出版社
HONG KONG ACADEMY OF MEDICINE PRESS

HONG KONG MEDICAL JOURNAL 香港醫學雜誌
Volume 30 Number 1 **February 2024**
SUPPLEMENT 1

Health and Medical Research Fund

Research Dissemination Reports

VISUAL SYSTEM

REPRODUCTIVE HEALTH

Editorial

Dissemination reports are concise informative reports of health-related research supported by the Health and Medical Research Fund administered by the Health Bureau. In this edition, we present 11 dissemination reports of projects related to infectious diseases, health services research, cancer, gastrointestinal disease, visual system, and reproductive health. In particular, research findings of three projects may provide insights to enhance clinical practices and help inform health policy formulation in Hong Kong.

Early prediction of an impending influenza outbreak would be very useful for mitigating potential public health implications, such as planning for surge capacity in public hospitals. Such prediction in sub-tropical regions like Hong Kong are difficult not least because the seasonal characteristics of influenza in temperate and tropical locations are quite different and real-time data on influenza infection dynamics are limited. Ali et al[1] attempted to forecast seasonal influenza transmission by integrating multiple surveillance streams on influenza transmissibility in Hong Kong. During the study period 1998-2020, 58 distinct influenza epidemics were identified. Associations between influenza transmissibility and mean ambient humidity and ambient ozone were observed. The mechanistic framework–based forecasting was found to be comparable with statistical framework–based forecasting.

Parkinson disease (PD) is a neurodegenerative disorder associated with motor and non-motor symptoms. Progression of non-motor and motor symptoms such as mood disturbances, cognitive impairment, sleep problems, fatigue, postural instability, and gait disturbance further contribute to disability and reduced quality of life. Mak et al[2] evaluated the effects of a 26-week combined balance exercise and brisk walking programme, compared with flexibility and strengthening exercise, on improving non-motor and motor symptoms among 99 Chinese people with mild-to-moderate PD. They found that the intervention reduces non-motor and motor symptoms and enhances balance and walking capacity immediately post-training, with positive carry-over effects for all outcomes except non-motor symptoms at 6-month follow-up. Exercise compliance was good and adverse effects were minimal. Thus, a combined balance and brisk walking programme has the potential to modify the progression of PD.

Exercise training is an important component of cardiac rehabilitation (CR) for patients with coronary heart disease (CHD). However, compliance with CR is challenging. Thus, making exercise practical, achievable, and enjoyable would help patients with CHD maintain physical activity. Chair et al[3] examined the effects and cost-effectiveness of a 2-week music-paced physical activity intervention conducted as part of an 8-week CR programme on cardiac health outcomes among 130 Chinese adult patients with CHD. The music-paced physical activity intervention was more effective, compared with usual care, in terms of improvements in exercise capacity and exercise self-efficacy but was more expensive in terms of improving quality-adjusted life years, while the intervention was cost-effective based on the World Health Organization standard (ie, incremental cost-effectiveness ratio <3 times the gross domestic product per capita). This study provided evidence that the application of music into exercise training may lead to positive changes in exercise capacity in the short-term and exercise self-efficacy in the long-term.

Supplement editors

Dr Anne Fung
Head
Research and Data Analytics Office
Health Bureau

Dr Richard A Collins
Senior Scientific Reviewer
Research and Data Analytics Office
Health Bureau

References

1. Ali ST, Wu P, He D, Tian L, Cowling BJ. Forecasting influenza epidemics in Hong Kong using multiple streams of syndromic and laboratory surveillance data: abridged secondary publication. Hong Kong Med J 2024;30(Suppl 1):S4-8.
2. Mak KYM, Cheung THR, Ho SL. Combined balance and brisk walking training to improve motor and non-motor symptoms in people with Parkinson disease: abridged secondary publication. Hong Kong Med J 2024;30(Suppl 1):S16-7.
3. Chair SY, Sit JWH, Wong EML, et al. Music-paced physical activity intervention for patients with coronary heart disease: abridged secondary publication. Hong Kong Med J 2024;30(Suppl 1):S18-22.

Forecasting influenza epidemics in Hong Kong using multiple streams of syndromic and laboratory surveillance data: abridged secondary publication

ST Ali *, P Wu, D He, L Tian, BJ Cowling

KEY MESSAGES

1. This study provided an integrated framework to identify potential drivers of influenza transmission in terms of associations and the ability to forecast the intensity (attack rate and peak magnitude) and the peak timing of influenza epidemics in Hong Kong.
2. Ability to predict influenza epidemic outcomes in a timely manner is instrumental in assisting public health planning strategies and assessing the effects of interventions.

Hong Kong Med J 2024;30(Suppl 1):S4-8
HMRF project number: 18171202

[1] ST Ali, [1] P Wu, [2] D He, [1] L Tian, [1] BJ Cowling

[1] *School of Public Health, Li Ka Shing Faculty of Medicine, The University of Hong Kong, Hong Kong SAR, China*
[2] *Department of Applied Mathematics, The Hong Kong Polytechnic University, Hong Kong SAR, China*

* Principal applicant and corresponding author: alist15@hku.hk

Introduction

Forecasting influenza outbreaks is a challenging task because even two consecutive annual outbreaks of the same virus can have very different impacts. Furthermore, the seasonal characteristics of influenza differ between temperate and tropical locations. In Hong Kong, a sub-tropical city, influenza epidemics can occur at any time of year, with a peak in winter almost every year and a second peak in spring, summer, or autumn in many years.[1] The lack of real-time dynamics and characteristics of epidemics adversely affects public health planning. For example, hospitals may suddenly experience a surge in influenza cases without warning or adequate preparation.

We previously found that absolute humidity and ambient ozone were associated with influenza transmissibility in Hong Kong.[2] The comparative results of two diverse modelling frameworks could represent advances in the real-time forecasting (short-term and long-term) of influenza incidence (or attack rate), peak timing, and peak intensity in Hong Kong (Fig 1).[1] We aimed to forecast seasonal influenza transmission and the effects of extrinsic driving factors in Hong Kong. We hypothesised that (1) real-time forecasting could be improved by integrating multiple surveillance data streams concerning influenza transmissibility in Hong Kong and that (2) the inclusion of driver data from multiple streams plus their predicted associations with influenza transmission could improve forecast accuracy and reduce uncertainty. We also assessed the effects of public health and social measures for COVID-19 on influenza dynamics in Hong Kong.

Methods

We retrieved weekly records of the influenza-like illness (ILI) consultation rate and proportion of specimens testing positive for influenza virus from the Centre for Health Protection of Hong Kong for the period 1998 to 2020. We then estimated the ILI+ proxy, a measure of influenza virus activity in the community.[2] We also retrieved daily mean meteorological variables and pollutants from the Hong Kong Observatory and the Hong Kong Environmental Protection Department, as well as the timing of school holidays along with school closures in response to epidemics/pandemics in Hong Kong.

We first identified potential drivers of influenza transmissibility and their associations. Transmissibility was measured by the instantaneous reproduction number (R_t), defined as the mean number of secondary infections caused by a typical single infectious person at time t. We estimated R_t from daily ILI+ proxy using a simple branching process model. We used R_t to derive an alternative measure of transmissibility, the transmission rate (β_t), which was strongly influenced by susceptibility depletion. We performed regression analysis with R_t and β_t to investigate the association between influenza transmissibility and each driver (meteorological, pollutant-related, and social) in Hong Kong.[2,3]

Using a generalised linear model with a log-link function, we assumed that the ILI+ proxy followed a negative binomial distribution with expected ILI+ proxy $\lambda(t + k)$ for the following k weeks, with $k \in (0,1,2,3)$ at week t. We constructed possible predictive model variants by incorporating various

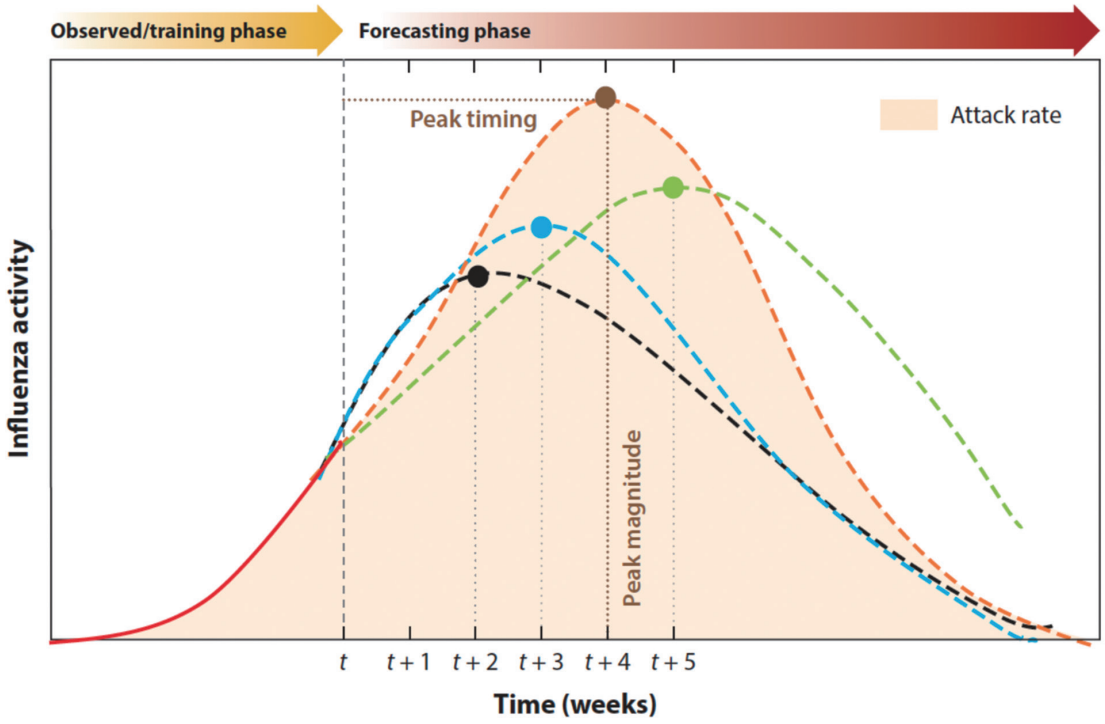

FIG 1. Forecasts of four different models in terms of peak timing, peak magnitude, and attack rate

combinations of drivers in the model, along with a periodic cubic spline basis in the base model. We conducted 10-fold cross-validation to assess model prediction performance for the period 2010 to 2019 (avoiding the 2009 swine flu pandemic) to select the best predictive model for short-term forecasting (1-4 weeks ahead) in 2020. Model variants were validated and ranked using weighted interval score, root mean square error, root mean square log error, mean absolute error, and mean rank. The model with the lowest weighted interval score was selected for further influenza forecasting beginning in the 3rd week of January 2020. We then constructed a predictive model for long-term forecasting (up to 52 weeks ahead) of influenza activity in 2020.

We constructed a general susceptible-vaccinated-exposed-infectious-recovered-susceptible compartmental model, which included seasonal vaccination, waning immunity, population demography, sociodemographic factors, and seasonal factors. We hypothesised that the transmission rate $\beta(t)$ is modulated by drivers such as seasonality (using a spline or standard periodic function), climatic factors, pollutants, sociodemographic factors, and noise driven by other extrinsic factors. Model variants with various combinations of drivers were constructed, as were their effective forms of association with $\beta(t)$ identified in the exploratory data analysis. We developed a problem-based inferential framework using the Markov chain Monte Carlo method to obtain the joint posterior distribution of model parameters with the adaptive Metropolis-Hastings algorithm, which was implemented with four chains; each chain included 100 000 iterations with a burn-in period of 30 000 iterations. Forecasting performances of the different models were determined by temporal cross-validation using the inferential approach with different training periods: 8, 6, and 4 years. The model with the lowest mean rank was selected for further forecasting with uncertainty (95% prediction interval [PI]) beginning in the 3rd week of January 2020.

The impact of public health and social measures for COVID-19 pandemic on seasonal influenza transmission was significant.[4] In Hong Kong, such measures were well-established by the 3rd week of January 2020. We compared the long-term forecasts of influenza cases and observed cases in 2020 to quantify the impact of the COVID-19 pandemic. We evaluated attack rates and peak magnitude for the winter-spring period (December 2019 to March 2020), the summer period (May 2020 to September 2020), and the whole 2019/20 season (October 2019 to September 2020); these periods corresponded to winter, summer, and seasonal epidemics,

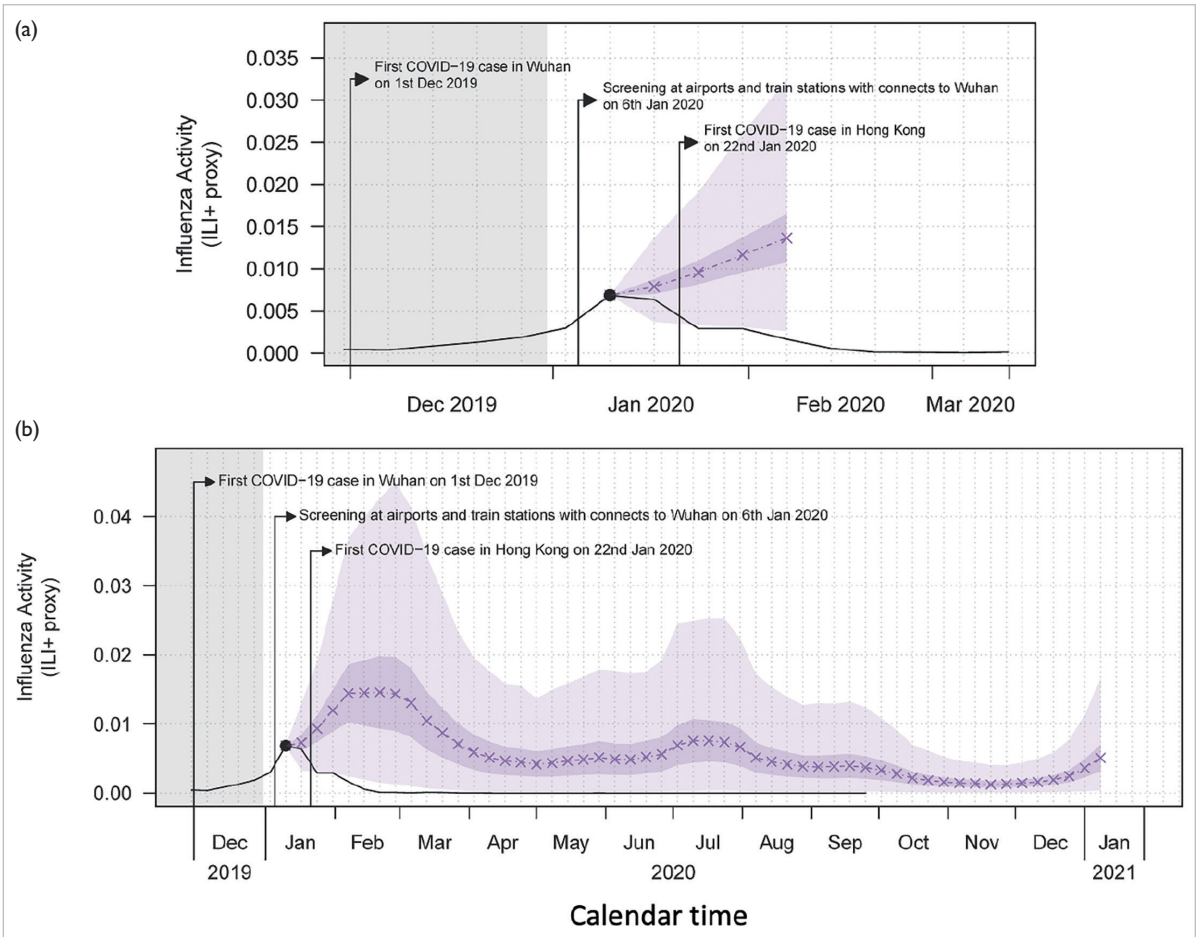

FIG 2. Statistical framework–based (a) short-term (1-4 weeks ahead) and (b) long-term (1-52 weeks ahead) forecasts beginning in the 3rd week of January 2020 in Hong Kong
Abbreviation: ILI+, influenza-like illness positive

respectively.[3] This mechanistic framework enabled fitting the observed influenza data from 2020 and quantifying the impact on transmissibility by evaluating reductions in transmission rate and number of cases related to the public health and social measures for COVID-19.

Results

Influenza viruses circulated annually, with peaks during January to March and July to September in most years. Over the entire study period of 1300 weeks, 1056 (81%) weeks were identified to be influenza epidemic, with 58 distinct influenza epidemics (types/subtypes). We observed changes in the seasonal patterns of annual influenza activity before, during, and after pandemics and epidemics (including swine flu pandemic in 2009, SARS epidemic in 2003, and COVID-19 pandemic). We found nonlinear associations of influenza transmissibility (R_t and β_t) with mean absolute humidity (U-shaped) and ambient ozone (negative power form) in Hong Kong. The U-shaped association with absolute humidity partially mimicked the winter and summer epidemics in sub-tropical areas. These extrinsic drivers were significant and could explain up to 18% of variation in the transmissibility.

The mechanistic framework–based forecast was comparable with the statistical framework–based forecast (Figs 2 and 3). Beginning in the 3rd week of January 2020, the short-term forecast (1-4 weeks ahead) of incidence reached 1.4% (95% PI=0.3%-3.4%) in the 1st week of February. Under the counterfactual scenario without the effects of public health and social measures for COVID-19, the long-term forecast suggested that a winter-spring influenza epidemic with a peak on the 16th to 22nd of February 2020 could have appeared, followed by a summer epidemic with a smaller peak on the 19th to 25th of July 2020. The winter-spring epidemic (December 2019 to March 2020) would have peaked with a weekly incidence of 1.5% (95% PI=0.2%-4.4%) and an attack rate of 14.4% (95% PI=9.4%-20.9%). In contrast, the summer epidemic (May 2020 to September 2020) would have had a lower incidence

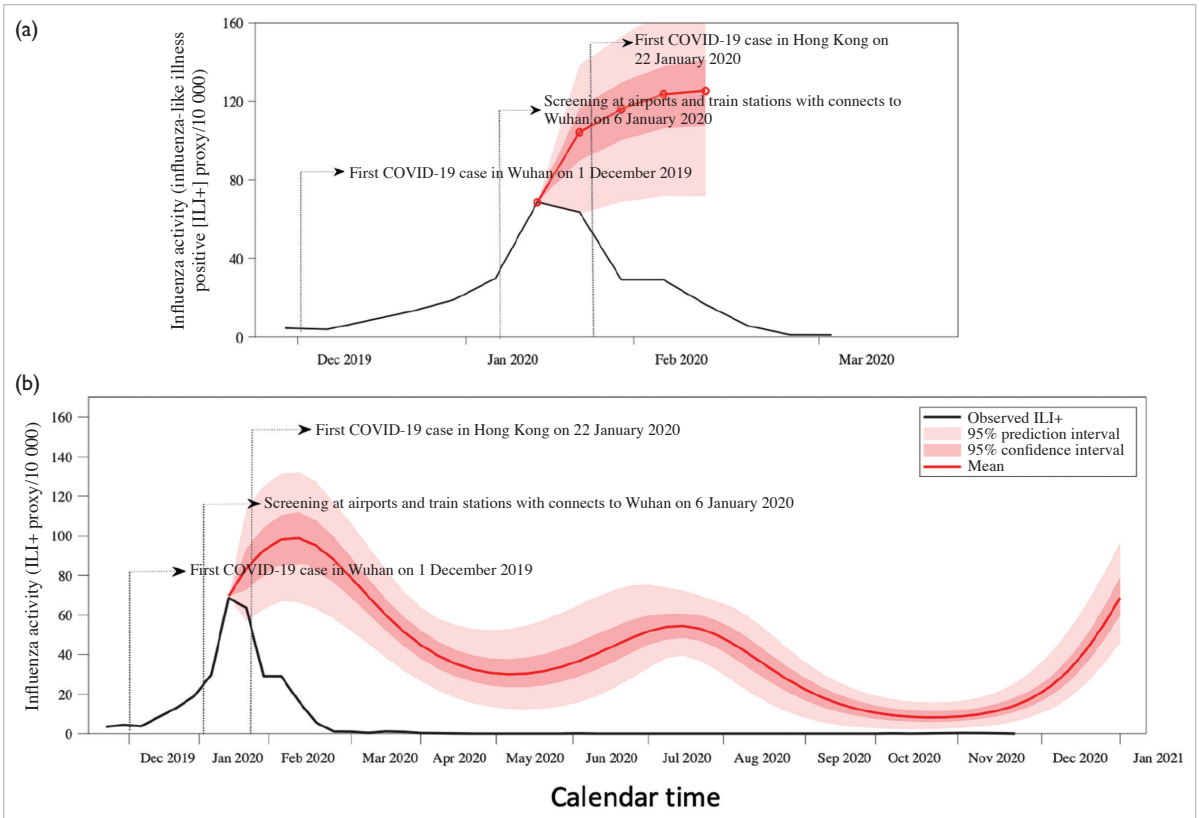

FIG 3. Mechanistic framework–based (a) short-term (1-4 weeks ahead) and (b) long-term (1-52 weeks ahead) forecasts beginning in the 3rd week of January 2020 in Hong Kong

and attack rate. The overall attack rate in the 2019/20 season was estimated to be 27.7% (95% PI=21.0%-35.7%), whereas the median attack rate was 23.7% (range, 11.5%-36.8%) between 2011/12 and 2018/19. The mechanistic framework–based forecast was more robust, with smaller uncertainty bounds (Figs 2 and 3).

Using the statistical framework, COVID-19 public health and social measures potentially led to a reduction of 87.9% (95% PI=84.1%-90.6%) in attack rate during the 2019/20 season. Similarly, the mechanistic framework estimated a reduction of 50.0% (95% credible interval=41.8%-59.9%) in transmissibility.

Discussion

Unlike temperate regions where influenza epidemics show strong seasonality during the winter period, tropical and sub-tropical regions show year-round influenza activity.[1] Thus, it is challenging to forecast influenza activity in tropical and sub-tropical regions. We found that both the statistical and mechanistic frameworks were comparable in terms of forecasting attack rate, peak magnitude, and peak timing in a timely manner. This finding is instrumental in assisting public health planning strategies.

Ambient ozone concentrations and school holidays/closures were significant drivers of short-term forecasts, whereas absolute humidity (with a U-shaped association) was the most important driver of long-term forecasts.[3] This indicated that low absolute humidity was associated with influenza transmission in temperate regions,[1] whereas low and high absolute humidity were associated with influenza transmission in tropical regions.[3] The negative associations between ozone concentration and influenza activity/transmissibility could explain the enhanced immunity against influenza virus infection observed under high ozone concentrations.[2]

The 3rd week of January 2020 was chosen as the first week of forecasting because there was no sustained influenza activity during that week in Hong Kong. We forecasted an attack rate of 27.7% in the 2019/20 season, which is close to the median attack rate of 23.7% in preceding seasons (2011/12 to 2018/19). Importantly, our frameworks could forecast outcomes in real time, as demonstrated in the annual national-level influenza forecasting competition "Predict the Influenza Season Challenge" at the United States Centers for Disease Control and Prevention.[5]

There were limitations in the present study.

First, the ILI+ proxy parameter was influenced by health-seeking behaviour and laboratory surveillance capacity, which could have been suppressed during the COVID-19 pandemic. Second, we could not stratify the analysis according to influenza virus subtype because no such information was available. Third, evolution (antigenic drift and shift) of influenza virus over time was not considered.

Funding

This study was supported by the Health and Medical Research Fund, Health Bureau, Hong Kong SAR Government (#18171202). The full report is available from the Health and Medical Research Fund website (https://rfs2.healthbureau.gov.hk).

Disclosure

The results of this research have been previously published in:

1. Ali ST, Cowling BJ, Wong JY, et al. Influenza seasonality and its environmental driving factors in mainland China and Hong Kong. Sci Total Environ 2022;818:151724.

2. Ali ST, Cowling BJ. Influenza virus: tracking, predicting and forecasting. Annu Rev Public Health 2021;42:43-57.

References

1. Ali ST, Cowling BJ. Influenza virus: tracking, predicting, and forecasting. Annu Rev Public Health 2021;42:43-57.
2. Ali ST, Wu P, Cauchemez S, et al. Ambient ozone and influenza transmissibility in Hong Kong. Eur Respir J 2018;51:1800369.
3. Ali ST, Cowling BJ, Wong JY, et al. Influenza seasonality and its environmental driving factors in mainland China and Hong Kong. Sci Total Environ 2022;818:151724.
4. Cowling BJ, Ali ST, Ng TWY, et al. Impact assessment of non-pharmaceutical interventions against coronavirus disease 2019 and influenza in Hong Kong: an observational study. Lancet Public Health 2020;5:e279-e288.
5. Biggerstaff M, Alper D, Dredze M, et al. Results from the Centers for Disease Control and Prevention's predict the 2013-2014 Influenza Season Challenge. BMC Infect Dis 2016;16:357.

Single amino acid substitution and inter-species transmission of MERS-coronavirus from camels to humans: abridged secondary publication

JSM Peiris *, RTY So, LLM Poon, KW Chu, CKP Mok, J Zhao

KEY MESSAGES

1. Middle East respiratory syndrome coronavirus (MERS-CoV) acquires a human-adaptive mutation in the nsp6 gene following inter-species transmission from camels to humans.
2. The nsp6 L232F mutation is associated with increased viral replication competence in the respiratory tracts of humans and mice.
3. The nsp6 L232F mutation affects autophagic machinery within host cells, thereby modifying viral replication competence.
4. MERS-CoV remains a public health threat, and ongoing surveillance in camels and humans is warranted.

Hong Kong Med J 2024;30(Suppl 1):S9-15
HMRF project number: 19181032

[1] JSM Peiris, [1] RTY So, [1] LLM Poon, [1] KW Chu, [1] CKP Mok, [2] J Zhao

[1] *School of Public Health, The University of Hong Kong, Hong Kong SAR, China*
[2] *State Key Laboratory of Respiratory Disease, Guangzhou, China*

* Principal applicant and corresponding author: malik@hku.hk

Introduction

Middle East respiratory syndrome coronavirus (MERS-CoV) was first identified as a cause of severe acute respiratory disease in humans in 2012. MERS-CoV remains a potential pandemic threat and a research priority.[1] Inter-species transmission of MERS-CoV from camels to humans is sporadic, possibly through direct or indirect camel contact. Clusters of human cases have been reported, typically in healthcare settings. Inter-species virus transmission from animals to humans is often associated with mutations as the virus attempts to adapt to the new host. A classic example is the adaptative mutation of E627K, which arose in the PB2 gene of avian influenza A virus following transmission to humans.[2] We aimed to identify and characterise host adaptive mutations that emerge when MERS-CoV is transmitted from camels to humans.

Methods

MERS-CoV sequences (full genome and >20 kb) were retrieved. Sequences were aligned using MAFFT and processed for phylogenetic analysis. A bacterial artificial chromosome plasmid construct of the infectious MERS-CoV/China01(GD01) strain was provided by Guangzhou Medical University.

An independent risk assessment of the genetic modification of MERS-CoV was implemented in the Safety Office, the University of Hong Kong. The experiment envisaged was a loss-of-function mutation as we started from a human virus possessing the putative 'human adaptive mutation' to mutate nsp232 to the camel genotype. Thus, the genetic modification procedure did not increase the risk for humans. All handling of infectious virus was carried out at bio-safety level 3 containment.

The GD01 human strain of MERS-CoV exhibits the L232F mutation in the nsp6 gene. We rescued a recombinant GD01 with and without the nsp6 L232F mutation using our previously described methods.[3] Rescued viruses were plaque-purified in Vero cells and subcultured in Huh-7 cells to generate virus stocks, which were aliquoted and stored at -80°C. The genetic identities of the virus stocks were confirmed, and the titre of each virus stock was determined. We characterised the replication kinetics of the two isogenic mutants with the nsp6 L232F mutation using our previously described methods.[3] Cellular RNA was extracted from virus-infected cells. Purified RNA was reverse-transcribed into cDNA using random hexamers and then subject to gene expression. Vero cells were fixed in 10% formalin and processed for transmission electron microscopy. The effect of MERS-CoV infection on autophagic flux was determined by transfection of a tandem-EGFP-mCherry-LC3 reporter plasmid encoding fluorescent LC3, which is detectable as yellow puncta in autophagosomes (APs) and as red puncta in autolysosomes (ALs). Chloroquine and BafA1 were used as controls for the inhibition of autophagic flux. Vero cells were transfected with Lipofectamine 2000 and then infected with MERS-CoV at a multiplicity of infection (MOI) of 0.01.

Results

We retrieved 502 complete and partial (>20 kb) MERS-CoV genomes from GenBank, which comprised both the Arabian Peninsula clade A/B and Africa clade C sequences. We used these genomes to identify mutations that are more likely to occur in human MERS-CoV. Using the Fisher's exact test adjusted with Bonferroni correction, 11 mutations were significantly more frequent to occur in MERS-CoV sequences from humans than from camels. These mutations were present in nsp3, nsp5, nsp6, nsp13, spike, and nucleocapsid viral proteins. Among these 11 mutations, the top hit (ie, the mutation with the greatest difference in occurrence between human and camel origin sequences) was the leucine (Leu L) to phenylalanine (Phe F) mutation at codon 232 of the nsp6 protein, which occurred in 60 (25.2%) of 238 human sequences but in 1 (0.4%) of 264 camel sequences (from clade B). To visualise the nsp6 mutation in the MERS-CoV phylogeny, we constructed a phylogenetic tree of MERS-CoV sequences exhibiting the nsp6 mutation genotype in human and camel hosts (Fig 1).

The nsp6 L232F mutation did not alter replication in Calu-3 or Huh-7 cells, but it enhanced replication in Vero cells (Fig 2). The isogenic mutant rGD01-nsp6 232L displayed smaller plaque sizes compared with rGD01-WT, which contains nsp6 232F (1 vs 0.71, P<0.001). These data suggest that the nsp6 L232F mutation increases viral replication. We confirmed this enhanced viral replication competence by a competitive growth assay involving co-culture with different ratios (9:1, 1:1, and 1:9) of rGD01-WT and rGD01-nsp6 232L. We measured the genotype frequencies after various numbers of viral passages in Vero cells (data not shown). After three passages, a distinct nsp6 Phe genotype was observed at all co-culture ratios in Vero cells, implying that rGD01-WT has more robust intrinsic replication kinetics (data not shown). No competitive advantage was observed in Calu-3 cells.

Triplicate cultures were infected with each of the isogenic viruses. In bronchial cultures, rGD01-nsp6 232L exhibited significant reduction of replication at 48 and 72 hours post-infection (hpi) [Fig 2]. Replication did not significantly differ in lung cultures, reflecting a phenotype similar to the results in Calu-3 lung adenocarcinoma cells.

After intranasal inoculation of 10^4 plaque-forming units of virus per mouse, we observed significantly lower titres of rGD01-nsp6 232L virus at 1 to 3 days post-infection (dpi); the greatest difference of 1.71 log10 median tissue culture infectious dose ($TCID_{50}$)/mL was observed on day 1 (Fig 2). We also detected lower amounts of subgenomic viral RNA from rGD01-nsp6 232L at 1 to 3 dpi. These findings suggest that the nsp6 L232F mutation enhanced replication in mouse lung tissue.

Protein levels of pro-inflammatory cytokines and chemokines in the lungs were measured from 4 hpi to 5 dpi. Although both viruses exhibited detectable replication at 1 dpi, there was no significant induction of inflammatory markers compared with mock infection controls (data not shown). These results suggest that effective innate immune antagonism was achieved by both viruses, which is an expected phenotype for MERS-CoV infection. At 2 to 3 dpi, the protein levels of monocyte chemoattractant protein-1, interferon gamma-induced protein-10, and interleukin-6 in mouse lungs were significantly higher upon infection with rGD01-WT than upon infection with rGD01-nsp6 232L. Considering that rGD01-WT had a higher viral load in the lungs compared with rGD01-nsp6 232L at 2 to 3 dpi, the increased innate immune response may reflect the higher viral load in the lungs, rather than the involvement of the nsp6 L232F mutation in immune antagonism.

The nsp6 protein has previously been implicated in AP restriction.[4] Using a tandem fluorescent-tagged LC3 (mRFP-EGFP-LC3) reporter, autophagic flux can be measured based on pH differences between AP and AL environments; the more acidic AL environment quenches the EGFP signal. This reporter can quantify the numbers of autophagic compartments in infected cells. After Vero cells were transfected with mRFP-EGFP-LC3, we infected those cells with each of the two isogenic viruses at an MOI of 0.01 and measured the numbers of autophagic compartments at 24 hpi. There was no difference in AL number between cells infected with either isogenic virus, but the AP number was higher in rGD01-nsp232L-infected cells; thus, the camel Leu residue resulted in lower autophagic flux, indicated by less AP to AL fusion (Fig 3).

In a parallel approach, we conducted LC3 immunoblotting to measure autophagic flux. LC3 is a well-known autophagic marker that exists in two forms: LC3-I, found in the cytoplasm, and LC3-II, bound to the AP membrane. Changes in the LC3 immunoblotting band intensity ratio of LC3-II/actin (reflecting cellular AP level) in response to BafA1 (an inhibitor of AP to AL fusion) can provide information about autophagic flux. Among Vero cells infected at an MOI of 0.01, only rGD01-WT-infected cells exhibited an increase in the LC3-II/actin ratio upon treatment with BafA1 at 24 hpi, suggesting that rGD01-WT-infected cells had higher autophagic flux than rGD01-nsp6 232L-infected cells (Fig 3). At 48 hpi, both viruses blocked AP to AL fusion, indicated by the absence of BafA1-mediated changes in the LC3-II/actin ratio. We regarded LC3-I as a proxy for double-membrane vesicle (DMV) levels; rGD01-WT-infected cells showed higher levels of LC3-I compared with rGD01-nsp6 232L-infected

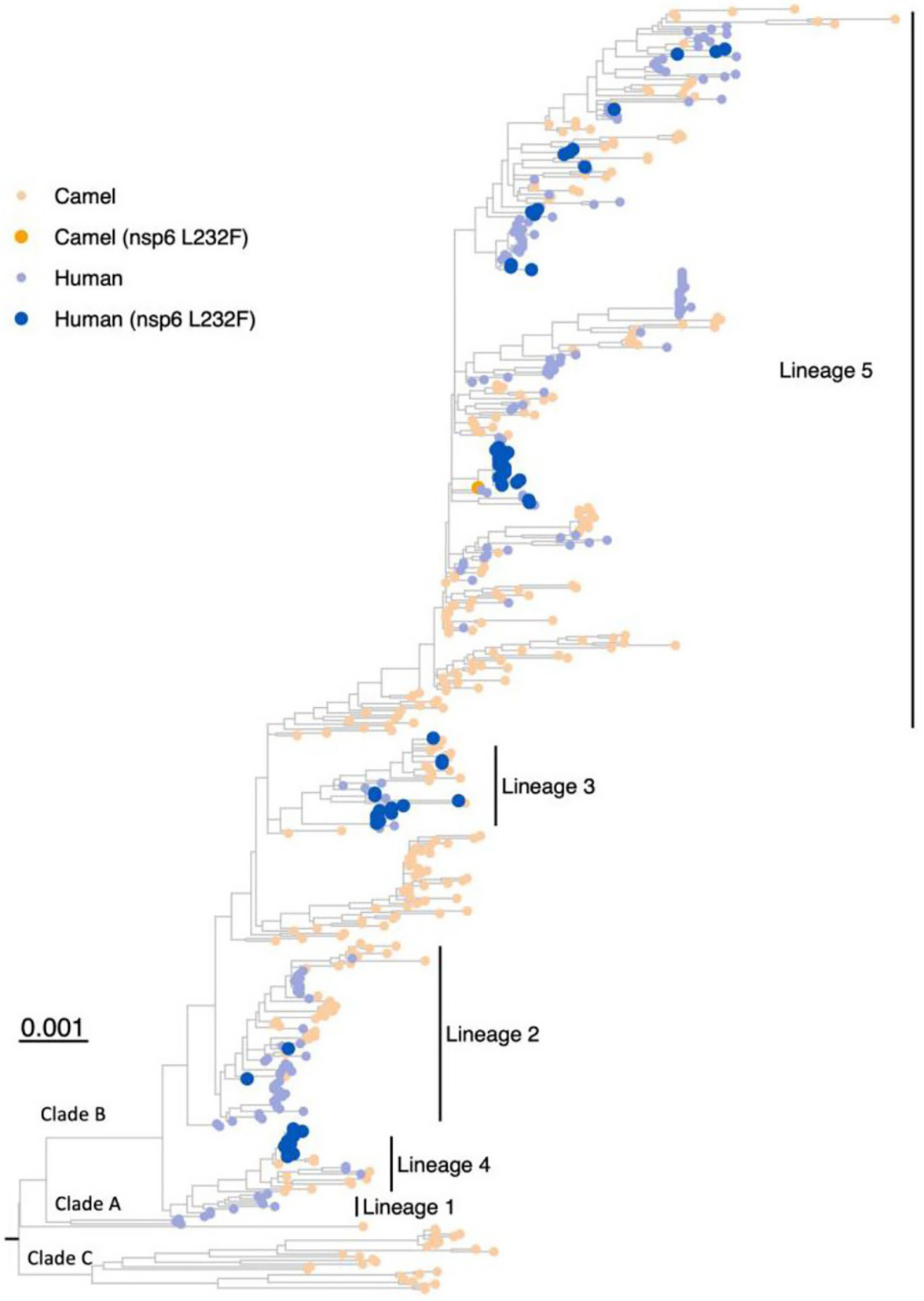

FIG 1. The Middle East respiratory syndrome coronavirus (MERS-CoV) nsp6 L232F mutation preferentially occurs in humans, compared with camels, in 502 complete and partial MERS-CoV genomes

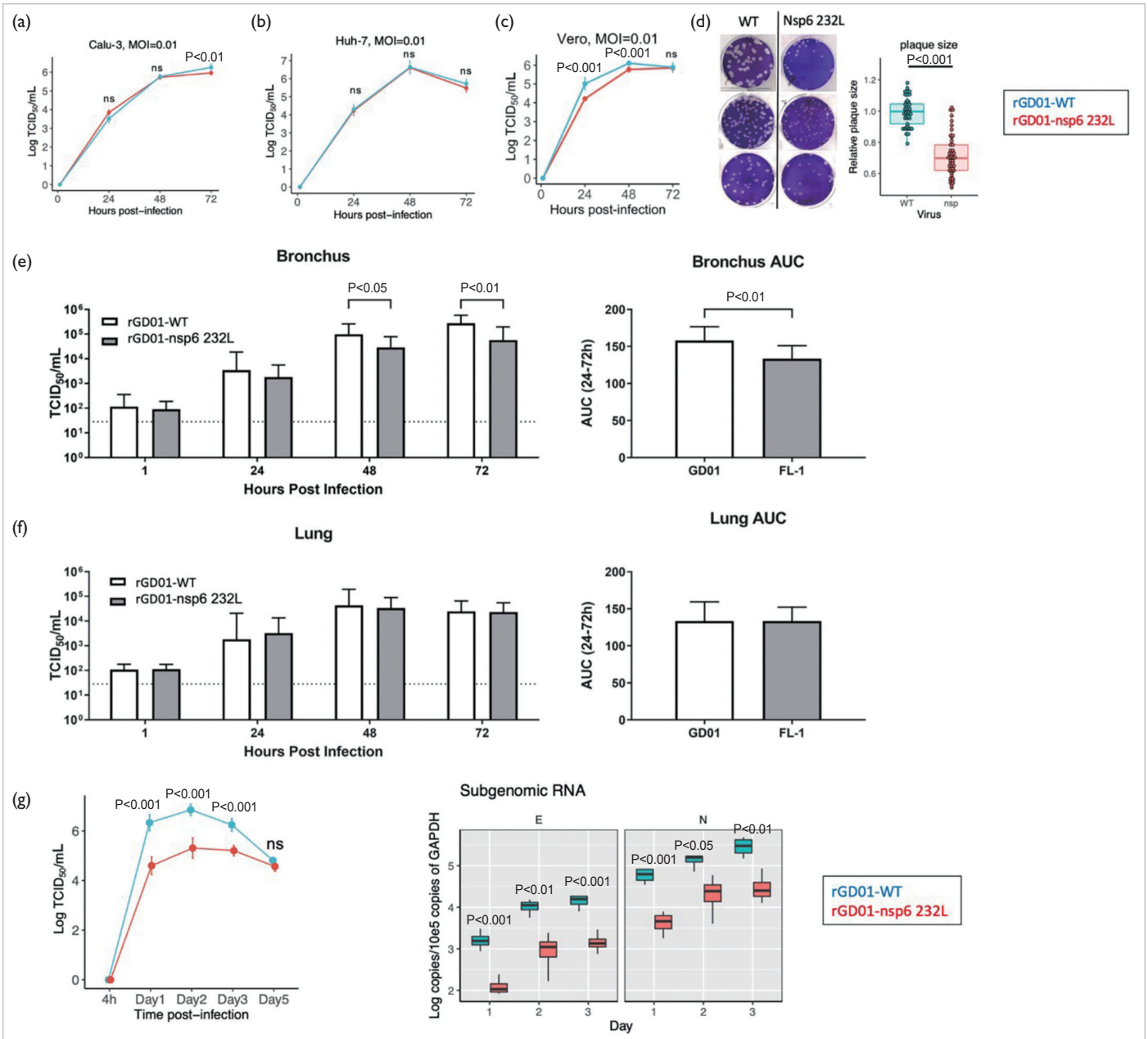

FIG 2. Viral replication kinetics of rGD01-WT and rGD01-nsp6 232L: (a) Calu-3 cells, (b) Huh-7 cells, and (c) Vero cells were infected at a multiplicity of infection (MOI) of 0.01. (d) Relative plaque sizes of rGD01-WT and rGD01-nsp6 232L viruses were determined in Vero cells. Viral replication kinetics in ex vivo cultures of human (e) bronchial and (f) lung tissues. The horizontal dotted line denotes the limit of detection in median tissue culture infectious dose ($TCID_{50}$) assays. (g) Viral replication kinetics in the lungs of human DPP4-knockin mice.

cells at both 24 and 48 hpi, indirectly suggesting that rGD01-WT infection led to higher numbers of DMV structures for viral RNA synthesis.

Nsp3, 4, and 6 reportedly induce the formation of DMV structures in an overexpression system. We used electron microscopy to measure the formation of DMV structures induced by each of the isogenic viruses. In Vero cells, single-membrane virus compartment vesicles containing virions were observed for both viruses at 24 hpi, whereas distinct DMV structures were not evident (data not shown). Therefore, we could not quantify the difference in DMV formation induced by the two isogenic viruses. However, we observed a larger vesicle diameter and higher virion number in each vesicle in rGD01-WT-infected cells than in rGD01-nsp6 232L-infected cells, confirming that rGD01-WT induces greater viral production.

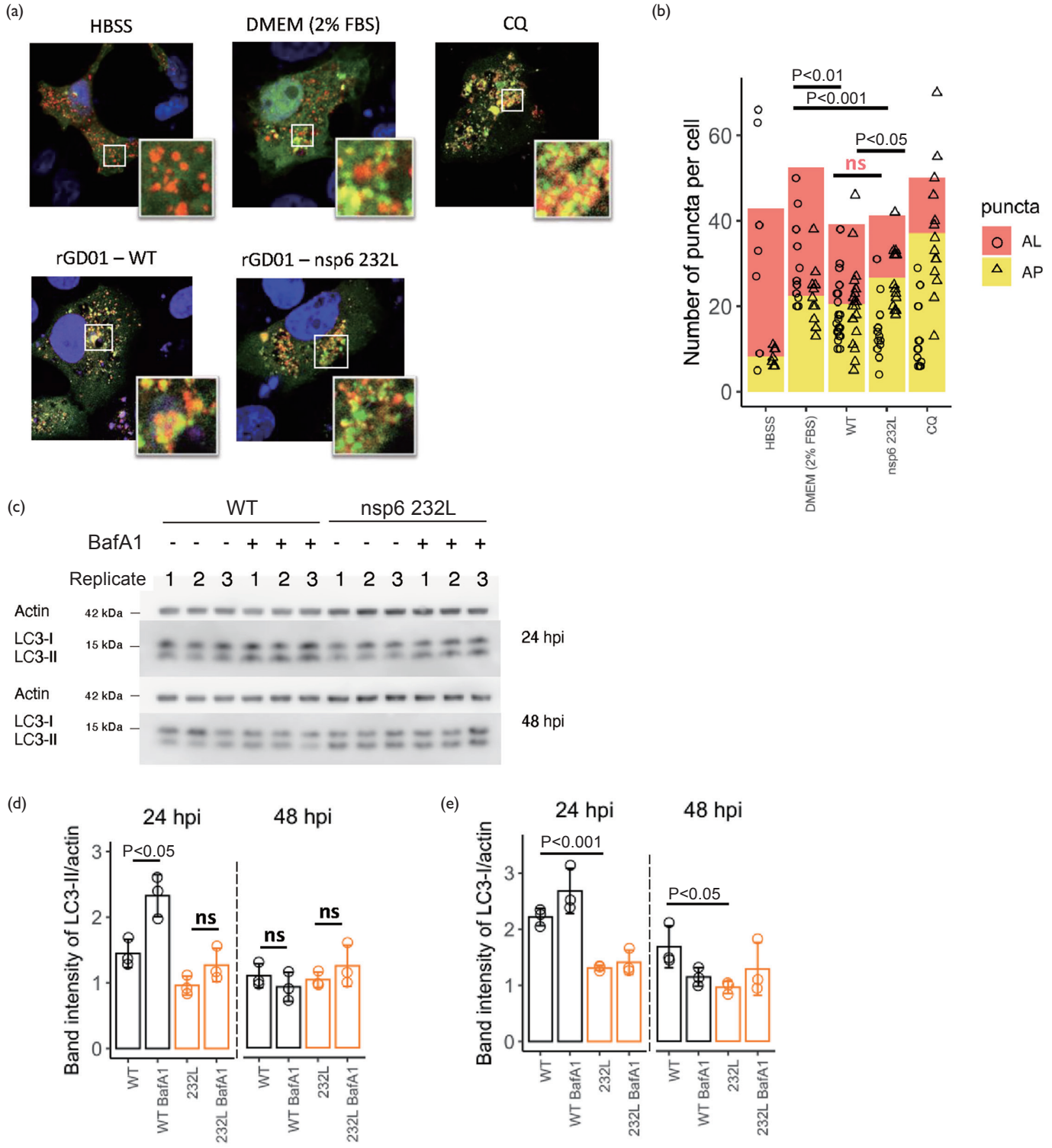

FIG 3. The nsp6 L232F mutation modulates autophagy and double-membrane vesicle quantity. (a) Vero cells transfected with mCherry and EGFP-tagged LC3 were infected with each of the two viruses at a multiplicity of infection (MOI) of 0.01 and subjected to immunofluorescence measurements. Hanks' Balanced Salt Solution (HBSS)-mediated induction of cell starvation served as the high autophagic flux control, Dulbecco's modified Eagle medium (DMEM) supplemented with 2% fetal bovine serum (FBS) served as the basal autophagic flux control, and chloroquine (CQ, 100 mM)-mediated inhibition of autophagosome (AP) to autolysosome (AL) fusion served as the low autophagic flux control. (b) Summary statistics of the numbers of AP and AL puncta counted. (c) Immunoblotting of LC3-I/II in Vero cells infected at an MOI of 0.01. To block AP to AL fusion, cells were incubated with BafA1 (0.1 μM) for 2 hours before collection of protein lysates. Band intensity of (d) LC3-II/actin ratio (representing AP level) and (e) LC3-I/actin ratio (representing a proxy measurement of double-membrane vesicle level).

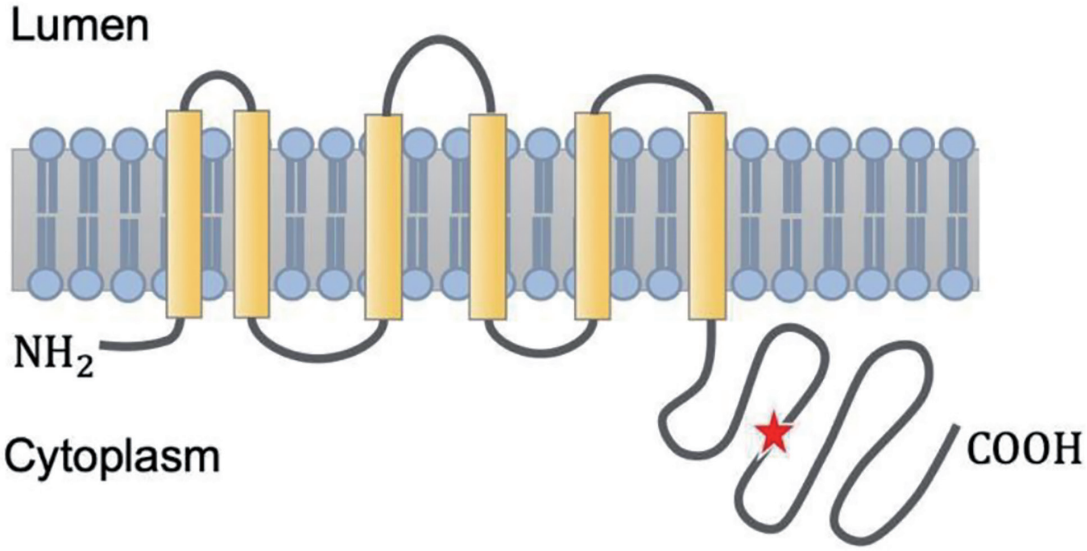

FIG 4. Membrane topology of MERS-CoV nsp6 and the location of the L232F mutation.

Discussion

We compared MERS-CoV mutations in camels and humans, which revealed a potential adaptive mutation, nsp6 L232F, that preferentially occurred in humans. MERS-CoV nsp6 is a highly conserved non-structural protein among Betacoronaviruses that consists of six transmembrane domains and a trailing C-terminal domain in the cytoplasm. The L232F mutation identified is located at the C terminus of nsp6, which potentially alters the intrinsic function of nsp6 (Fig 4).

We used reverse genetics to explore the phenotypic effects of this mutation in recombinant isogenic viruses. Compared with a Leu residue that is present in most camel MERS-CoVs, the recurrent Phe residue mutation in human MERS-CoVs led to enhanced replication in Vero cells, ex vivo cultures of human bronchial tissue, and the human DPP4 mouse model. The underlying mutation did not cause significant changes in interferon antagonism in vitro.

We explored the mechanistic basis for the effects of the nsp6 L232F mutation on viral replication competence in human cells. We investigated its effects on cellular autophagy, as CoV nsp6 has been suggested to hijack autophagy machinery for viral replication and generation of DMV structures. Both isogenic viruses showed autophagic inhibition with fewer ALs. Furthermore, LC3-II immunoblotting showed that the nsp6 L232F mutation resulted in less AP accumulation and a higher autophagic flux. However, the physiologic consequences of this phenotype are unclear because CoV manipulation of autophagy is not fully understood. Additionally, LC3-I is reportedly associated with DMVs. Our data showed that rGD01-WT-infected cells exhibited higher levels of LC3-I compared with rGD01-nsp6 232L-infected cells, possibly reflecting the higher number of DMVs in rGD01-WT-infected cells and corresponding increase in viral production. Further experiments that involve immunofluorescence staining of dsRNA(+) LC3 (+) puncta could validate this hypothesis. Electron microscopy did not show distinct DMV structures at 24 hpi. However, virion-containing vesicles were more visible.

Conclusion

The amino acid substitution nsp6 L232F is associated with transmission of MERS-CoV to humans. This mutation confers a replication advantage to the virus in Vero cells, ex vivo cultures of human bronchial tissue, and experimentally infected mice. This mutation affects AP function, but its effects on viral replication competence or host adaptation remain unclear. Multiple studies have detected the nsp6 L232F mutation during the generation of mouse-adapted MERS-CoV strains through passage in mice.[5]

We identified a potential human-adaptive mutation in the nsp6 protein of human MERS-CoV, which increased viral replication competence in some models. Our findings illustrate the potential

for MERS-CoV to achieve greater viral fitness through repeated inter-species transmission from camels to humans. We recommend systematic serial sampling of specimens from MERS-infected humans to determine whether this nsp6 mutation becomes increasingly prevalent during the course of infection in humans.

Funding

This study was supported by the Health and Medical Research Fund, Health Bureau, Hong Kong SAR Government (#19181032). The full report is available from the Health and Medical Research Fund website (https://rfs2.healthbureau.gov.hk).

Disclosure

The results of this research have been previously published in:

1. So RTY, Chu DKW, Hui KPY, et al. Amino acid substitution L232F in non-structural protein 6 identified as a possible human-adaptive mutation in clade B MERS coronaviruses. J Virol 2023;97:e0136923.

References

1. Peiris M, Perlman S. Unresolved questions in the zoonotic transmission of MERS. Curr Opin Virol 2022;52:258-64.
2. Webster RG, Monto AS, Braciale TJ, Lamb RA, editors. Textbook of Influenza, 2nd Edition. Wiley: 2013; 157-71.
3. Zhou Z, Hui KPY, So RTY, et al. Phenotypic and genetic characterization of MERS coronaviruses from Africa to understand their zoonotic potential. Proc Natl Acad Sci U S A 2021;118:e2103984118.
4. Li K, Wohlford-Lenane CL, Channappanavar R, et al. Mouse-adapted MERS coronavirus causes lethal lung disease in human DPP4 knockin mice. Proc Natl Acad Sci U S A 2017;114:E3119-28.
5. Cottam EM, Whelband MC, Wileman T. Coronavirus NSP6 restricts autophagosome expansion. Autophagy 2014;10:1426-41.

Combined balance and brisk walking training to improve motor and non-motor symptoms in people with Parkinson disease: abridged secondary publication

KYM Mak *, THR Cheung, SL Ho

KEY MESSAGES

1. In patients with mild to moderate Parkinson disease, a 6-month combined balance and brisk walking programme improves motor and non-motor symptoms as well as balance and walking capacity, with carry-over effects at the 6-month follow-up for all outcomes (except non-motor symptoms).
2. Exercise adherence was good, and adverse events were few.
3. A combined balance and brisk walking programme can delay the progression of Parkinson disease.

Hong Kong Med J 2024;30(Suppl 1):S16-7
HMRF project number: 07183046

[1] KYM Mak, [2] THR Cheung, [3] SL Ho

[1] *Department of Rehabilitation Sciences, The Hong Kong Polytechnic University, Hong Kong SAR, China*
[2] *School of Health Sciences, Western Sydney University, Australia*
[3] *Department of Medicine, Queen Mary Hospital, Hong Kong SAR, China*

* Principal applicant and corresponding author: Margaret.Mak@polyu.edu.hk

Introduction

Parkinson disease (PD) is a neurodegenerative disorder associated with motor and non-motor symptoms that lead to functional disability and reduced quality of life. Pharmacological intervention is the mainstay management for motor symptoms, but its effects on most non-motor symptoms remain limited. Aerobic exercise can improve physical functions and motor symptoms in patients with PD. Combinations of balance, gait, and aerobic exercises can improve mobility, fatigue, anxiety, and sleep problems.[1,2] We compared a combined balance and brisk walking (BBW) exercise programme with a flexibility and strengthening exercise programme in terms of improvement in motor and non-motor symptoms among people with PD.

Methods

Patients aged >30 years with mild to moderate PD who could walk independently were recruited. Those with clinically significant neurological disorders (other than PD), musculoskeletal conditions or cognitive impairments were excluded. Participants were randomly assigned to either the BBW group or the control group for 6 months.

Participants in the BBW group received 10 sessions of BBW training supervised by physical therapists (involving large arm swings and long strides at a moderate to fast speed) targeted to achieve moderate intensity. Participants were instructed to perform 150 minutes of brisk walking per week. A smartwatch was used to monitor real-time changes in heart rate and exercise intensity as well as the duration of brisk walking.

Participants in the control group received training on flexibility, strength, and walking with good posture and stability. The active control programme was designed to provide a placebo effect and maintain motivation; it was considered superior to usual care without any intervention.

Results

The BBW group (n=49) and the control group (n=50) had comparable demographic and clinical outcomes at baseline. Compared with the control group, the BBW group exhibited greater decreases in Movement Disorder Society Unified Parkinson Disease Rating Scale motor and non-motor scores as well as greater increases in Mini-Balance Evaluation Systems Test score and 6-minute walk distance at treatment completion (all $P<0.001$). At the 6-month follow-up, the BBW group displayed greater improvement than the control group for all outcomes ($P=0.001$), except non-motor score. Both groups had high attendance rate of 95%. More than 70% of participants in the BBW group completed the recommended 150 minutes of moderate-intensity brisk walking per week. Six participants in the BBW group had mild back or knee pain during training.

Discussion

Aerobic exercise training can lead to clinically significant improvement of motor symptoms.[3] In the present study, the positive post-training effect but insignificant carry-over effect on non-motor symptoms could be related to the low baseline

values of participants. The significant improvements of balance performance and walking capacity could be attributed to task-specific balance and gait training. The combination of aerobic and balance exercises could have induced neuroplasticity such as increased dopamine release and neurotrophic factors.[4] These changes could lead to improvement of both motor and non-motor symptoms in patients with PD, which is associated with the reversal of disability progression in patients with PD. The use of real-time heart rate monitoring and weekly feedback from physical therapists could motivate and facilitate exercise adherence. These strategies could have empowered the participants in the BBW group to develop a regular exercise habit, leading to better 6-month outcomes.

Conclusion

In patients with mild to moderate PD, a combined BBW programme improves motor and non-motor symptoms as well as balance and walking capacity, with carry-over effects at 6-month follow-up for all outcomes (except non-motor symptoms).

Funding

This study was supported by the Health and Medical Research Fund, Health Bureau, Hong Kong SAR Government (#07183046). The full report is available from the Health and Medical Research Fund website (https://rfs2.healthbureau.gov.hk).

References

1. Wu PL, Lee M, Wu SL, et al. Effects of home-based exercise on motor, non-motor symptoms and health-related quality of life in Parkinson's disease patients: a randomized controlled trial. Jpn J Nurs Sci 2021:e12418.
2. Granziera S, Alessandri A, Lazzaro A, Zara D, Scarpa A. Nordic walking and walking in Parkinson's disease: a randomized single-blind controlled trial. Aging Clin Exp Res 2021;33:965-71.
3. de Almeida FO, Santana V, Corcos DM, Ugrinowitsch C, Silva-Batista C. Effects of endurance training on motor signs of Parkinson's disease: a systematic review and metaanalysis. Sports Med 2022;52:1789-815.
4. Li JA, Loevaas MB, Guan C, et al. Does exercise attenuate disease progression in people with Parkinson's disease? A systematic review with meta-analyses. Neurorehabil Neural Repair 2023;37:328-52.

Music-paced physical activity intervention for patients with coronary heart disease: abridged secondary publication

SY Chair *, JWH Sit, EML Wong, KC Leung, HY Cheng, Q Wang, KC Choi, DSF Yu, TSY Leung

KEY MESSAGES

1. The combination of music with exercise enhances short-term exercise capacity and long-term self-efficacy.
2. Music-paced physical activity intervention is more effective but more expensive than the usual care for improving quality-adjusted life years. The intervention is considered cost-effective based on World Health Organization criteria.
3. The information-motivation-strategy model and the self-determination theory are practical frameworks for motivating the maintenance of exercise behaviour.

Hong Kong Med J 2024;30(Suppl 1):S18-22
HMRF project number: 14152621

[1] SY Chair, [1] JWH Sit, [2] EML Wong, [3] KC Leung, [1] HY Cheng, [4] Q Wang, [1] KC Choi, [5] DSF Yu, [6] TSY Leung

[1] *The Nethersole School of Nursing, The Chinese University of Hong Kong, Hong Kong SAR, China*
[2] *School of Nursing, Tung Wah College, Hong Kong SAR, China*
[3] *Cardiac Rehabilitation and Resource Centre, Tung Wah Eastern Hospital, Hong Kong SAR, China*
[4] *School of Nursing, Shenzhen University, Shenzhen, China*
[5] *School of Nursing, The University of Hong Kong, Hong Kong SAR, China*
[6] *Physiotherapy, Tung Wah Eastern Hospital, Hong Kong SAR, China*

* Principal applicant and corresponding author: sychair@cuhk.edu.hk

Introduction

Exercise to promote cardiac rehabilitation (CR) is beneficial for patients with coronary heart disease (CHD). Nevertheless, exercise adherence is difficult to maintain after CHD onset. The combination of music with physical activity (PA) can enhance affective valence and physical performance, while reducing perceived exertion.[1] Memories and enjoyment induced by music are sources of intrinsic motivation for PA. Thus, music-paced PA may promote CR among patients with CHD.[2] We examined the cost-effectiveness and effects of music-paced physical activity (MPPA) on cardiac outcomes among patients with CHD.

Methods

This randomised controlled trial was conducted from August 2017 to September 2021. Patients with CHD aged ≥18 years participating CR at Tung Wah Eastern Hospital were recruited. Patients were excluded if they had physical impairment that prohibited exercise, cognitive impairment, a history of head trauma or seizure (contraindications to rhythmic auditory stimulation), or the inability to wear earbuds/headphones.

All participants completed the first 6 weeks of a CR programme at our centre to increase their exercise capacity. During weeks 7 and 8, the intervention group completed four sessions of MPPA, whereas the control group received the usual care.

In the intervention group, the information-motivation-strategy model[3] was used to motivate participants to perform moderate-intensity PA; personalised, tempo-synchronised music was used to enhance PA maintenance and clinical outcomes. A list of music with a pre-defined tempo (beats per minute [bpm]) was prepared for each patient to determine the range of bpm that the patient could use to achieve moderate intensity (60% to 75%) of maximum heart rate. Additionally, the self-determination theory[4] was applied during eight telephone calls to provide ongoing support for participants to make autonomous decisions on PA maintenance.

The control group completed four education sessions on performing moderate-intensity PA at home, along with telephone follow-up calls.

The primary outcome was exercise capacity in terms of 10-m incremental shuttle walk test. Secondary outcomes included exercise self-efficacy and self-determination, cost-effectiveness of the intervention, and clinical outcomes (eg, fasting blood glucose, haemoglobin A1c, total cholesterol, low-density and high-density lipoprotein cholesterol, triglycerides, blood pressure, waist circumference, body fat mass percentage and body mass index, high sensitivity C-reactive protein, PA level, and health-related quality of life [HRQoL]). PA level was evaluated using an accelerometer and the validated International Physical Activity Questionnaire-Short Form. Exercise self-efficacy was assessed using the validated Chinese version of the Cardiac Exercise Self-Efficacy Instrument. Exercise self-determination was evaluated using the Behavioural Regulation in

Exercise Questionnaire-3. Disease-specific HRQoL was measured using the 37-item Chinese version of the Cardiovascular Limitations and Symptoms Profile. The Chinese version of the EuroQol five dimensions questionnaire (EQ5-D) was used to analyse cost-effectiveness. Health-related costs were defined as direct medical and interventional costs. Outcomes were measured at baseline (T0), 3 months (T1), 6 months (T2), and 15 months (T3).

Bootstrapping and cost-effectiveness curves were plotted. Baseline characteristic homogeneity was compared between intervention and control groups using independent t-tests, the Chi-squared test, and Fisher's exact test, as appropriate. Generalised estimating equation models were used to compare differential changes at T1, T2, and T3 relative to T0 between the intervention and control groups. The intention-to-treat approach was used. Missing data were estimated using a model-based approach based on a quasi-maximum likelihood method.

Cost-effectiveness analyses were performed for total costs (medical + intervention/programme service costs) and incremental cost-effectiveness ratio (ICER), expressed as the incremental cost per quality-adjusted life year (QALY) gained over 15 months. The MPPA intervention was considered cost-effective if the ICER was <3 times the gross domestic product per capita (US$49 660.6 in 2021),[5] according to the World Health Organization.[6] The utility scores of EQ5-D at T0, T1, T2, and T3 were integrated using the trapezoidal method to calculate QALYs. All medical and programme service costs incurred were estimated for each participant using the method of Thompson and Barber, and the mean cost difference between intervention and control groups was used to derive the incremental total costs. A bias-corrected and accelerated bootstrapping method with 10 000 iterations was used to estimate 95% confidence intervals (CIs) for incremental total costs. The mean difference in QALYs between the two groups was regarded as the incremental effect.

TABLE 1. Baseline characteristics between the intervention and control groups and between the completer and dropout groups

Characteristic	Control (n=65)*	Intervention (n=65)*	P value	Completers (n=104)*	Dropouts (n=26)*	P value
Age, y	63.7±9.3	64.8±10.7	0.511	64.2±9.8	64.5±10.8	0.882
Sex						
Male	48 (73.8)	53 (81.5)	0.292	81 (77.9)	20 (76.9)	0.916
Female	17 (26.2)	12 (18.5)		23 (22.1)	6 (23.1)	
Marital status						
Single/divorced/separated/widowed	13 (20.3)	15 (23.8)	0.635	19 (18.8)	9 (34.6)	0.083
Married	51 (79.7)	48 (76.2)		82 (81.2)	17 (65.4)	
Education level						
Primary or below	13 (25.5)	16 (27.6)	0.946	26 (30.6)	3 (12.5)	0.019
Secondary	28 (54.9)	30 (51.7)		39 (45.9)	19 (79.2)	
Tertiary	10 (19.6)	12 (20.7)		20 (23.5)	2 (8.3)	
Have full/part-time job						
No	36 (56.3)	38 (58.5)	0.800	58 (56.3)	16 (61.5)	0.630
Yes	28 (43.8)	27 (41.5)		45 (43.7)	10 (38.5)	
Living alone						
No	49 (76.6)	57 (87.7)	0.099	87 (84.5)	19 (73.1)	0.249
Yes	15 (23.4)	8 (12.3)		16 (15.5)	7 (26.9)	
Type of housing						
Public	12 (19.0)	16 (25.0)	0.660	19 (18.6)	9 (36.0)	0.148
Subsidised	15 (23.8)	16 (25.0)		25 (24.5)	6 (24.0)	
Private	36 (57.1)	32 (50.0)		58 (56.9)	10 (40.0)	
Monthly family income, HK$						
<10 000	15 (23.8)	19 (29.7)	0.503	27 (26.7)	7 (26.9)	0.604
10 000-29 999	18 (28.6)	23 (35.9)		34 (33.7)	7 (26.9)	
≥30 000	21 (33.3)	16 (25.0)		30 (29.7)	7 (26.9)	
Receiving social assistance	9 (14.3)	6 (9.4)		10 (9.9)	5 (19.2)	

* Data are presented as mean ± standard deviation or No. (%) of participants

TABLE 2. Generalised estimating equation models for comparisons over time between the intervention and control groups in terms of cardiac outcomes

Variable	Regression coefficient (95% confidence interval)	P value	Regression coefficient (95% confidence interval)	P value	Regression coefficient (95% confidence interval)	P value	Regression coefficient (95% confidence interval)	P value
	10-m ISWT		CESEI total score		CLASP		EQ5-D VAS	
Group	-28.15 (-89.62 to 33.31)	0.369	-1.15 (-4.77 to 2.47)	0.534	-0.37 (-4.21 to 3.47)	0.851	3.60 (-1.95 to 9.15)	0.204
T1	-14.64 (-33.93 to 4.65)	0.137	-0.22 (-3.72 to 3.28)	0.900	-5.38 (-9.27 to -1.49)	0.007	3.07 (-0.63 to 6.76)	0.103
T2	-2.20 (-20.84 to 16.44)	0.817	1.54 (-0.91 to 3.99)	0.217	-0.98 (-4.37 to 2.42)	0.573	4.32 (-1.57 to 10.20)	0.150
T3	-21.48 (-43.41 to 0.44)	0.055	1.06 (-1.80 to 3.91)	0.468	-1.42 (-4.69 to 1.85)	0.395	3.95 (0.02 to 7.89)	0.049
Group×T1	35.68 (2.69 to 68.68)	0.034	3.95 (-0.63 to 8.54)	0.091	2.87 (-2.07 to 7.81)	0.256	-3.67 (-8.70 to 1.37)	0.154
Group×T2	26.94 (-7.44 to 61.31)	0.125	3.72 (0.11 to 7.32)	0.043	0.91 (-3.64 to 5.46)	0.695	-1.85 (-9.08 to 5.38)	0.616
Group×T3	13.08 (-24.43 to 50.59)	0.494	4.87 (0.95 to 8.79)	0.015	-1.00 (-5.52 to 3.51)	0.663	-0.96 (-6.45 to 4.53)	0.732
	Vigorous MET		Moderate MET		Walking MET		Total MET	
Group	1.62 (-5.54 to 8.79)	0.657	0.88 (-4.63 to 6.39)	0.755	1.88 (-4.58 to 8.33)	0.569	2.00 (-6.63 to 10.62)	0.650
T1	10.95 (0.90 to 21.00)	0.033	5.52 (-1.03 to 12.07)	0.098	2.71 (-2.72 to 8.13)	0.328	24.02 (14.50 to 33.54)	<0.001
T2	0.99 (-5.49 to 7.46)	0.766	7.77 (2.64 to 12.89)	0.003	7.81 (1.45 to 14.17)	0.016	10.75 (3.71 to 17.78)	0.003
T3	10.65 (3.78 to 17.51)	0.002	10.10 (3.15 to 17.04)	0.004	5.51 (-0.36 to 11.38)	0.066	13.25 (5.91 to 20.59)	<0.001
Group×T1	-4.78 (-17.03 to 7.47)	0.444	-3.21 (-11.43 to 5.01)	0.444	-2.03 (-10.22 to 6.16)	0.627	-4.93 (-17.94 to 8.08)	0.458
Group×T2	2.96 (-6.44 to 12.36)	0.537	-3.97 (-10.66 to 2.72)	0.244	-6.25 (-14.90 to 2.40)	0.157	-4.95 (-14.97 to 5.07)	0.333
Group×T3	7.65 (-6.14 to 21.45)	0.277	-3.69 (-12.60 to 5.23)	0.418	-0.98 (-9.42 to 7.46)	0.820	4.02 (-9.38 to 17.41)	0.557
	Amotivation		External regulation		Introjected regulation		Identified regulation	
Group	-0.04 (-0.30 to 0.22)	0.765	0.04 (-0.29 to 0.38)	0.810	-0.17 (-0.54 to 0.20)	0.370	0.03 (-0.20 to 0.26)	0.811
T1	2.46 (2.17 to 2.76)	<0.001	0.28 (-0.07 to 0.62)	0.113	0.11 (-0.22 to 0.45)	0.507	0.07 (-0.19 to 0.33)	0.601
T2	2.74 (2.44 to 3.05)	<0.001	0.12 (-0.20 to 0.43)	0.458	0.30 (-0.02 to 0.62)	0.069	0.23 (0.06 to 0.39)	0.007
T3	2.61 (2.32 to 2.89)	<0.001	0.17 (-0.14 to 0.48)	0.278	0.15 (-0.15 to 0.44)	0.330	0.06 (-0.14 to 0.26)	0.543
Group×T1	0.16 (-0.28 to 0.59)	0.477	-0.03 (-0.49 to 0.42)	0.886	0.24 (-0.23 to 0.70)	0.317	-0.01 (-0.34 to 0.31)	0.936
Group×T2	0.04 (-0.43 to 0.50)	0.870	-0.04 (-0.50 to 0.42)	0.853	0.14 (-0.32 to 0.60)	0.561	0.02 (-0.22 to 0.26)	0.888
Group×T3	0.03 (-0.41 to 0.48)	0.885	0.08 (-0.38 to 0.54)	0.731	0.36 (-0.10 to 0.81)	0.124	0.15 (-0.14 to 0.44)	0.303
	Integrated regulation		Intrinsic regulation					
Group	-0.09 (-0.40 to 0.23)	0.581	0.06 (-0.26 to 0.38)	0.717				
T1	0.36 (0.05 to 0.66)	0.022	0.26 (-0.01 to 0.52)	0.057				
T2	0.32 (0.08 to 0.56)	0.010	0.18 (-0.14 to 0.49)	0.268				
T3	0.21 (-0.05 to 0.48)	0.114	0.13 (-0.10 to 0.37)	0.269				
Group×T1	0.02 (-0.42 to 0.45)	0.945	0.08 (-0.32 to 0.48)	0.690				
Group×T2	0.07 (-0.33 to 0.46)	0.744	-0.02 (-0.47 to 0.42)	0.915				
Group×T3	0.13 (-0.29 to 0.55)	0.541	0.32 (-0.06 to 0.70)	0.101				
	Body weight		BMI		Waist circumference		Body fat	
Group	-0.27 (-3.84 to 3.31)	0.884	0.04 (-1.15 to 1.22)	0.954	-0.01 (-3.01 to 2.99)	0.993	-0.21 (-2.34 to 1.92)	0.849
T1	0.32 (-1.09 to 1.73)	0.660	0.30 (-0.24 to 0.84)	0.280	1.68 (0.19 to 3.17)	0.027	2.62 (1.31 to 3.93)	<0.001
T2	0.86 (-0.55 to 2.27)	0.230	0.52 (0.00 to 1.05)	0.050	0.99 (-0.47 to 2.46)	0.185	2.84 (1.60 to 4.08)	<0.001
T3	0.73 (-0.62 to 2.08)	0.288	0.37 (-0.13 to 0.87)	0.147	0.46 (-1.17 to 2.08)	0.582	2.07 (0.82 to 3.33)	0.001
Group×T1	-0.28 (-1.93 to 1.36)	0.736	-0.19 (-0.85 to 0.47)	0.572	-1.08 (-2.98 to 0.82)	0.264	-1.19 (-2.82 to 0.44)	0.153
Group×T2	-0.74 (-2.41 to 0.92)	0.381	-0.46 (-1.08 to 0.15)	0.140	-1.24 (-3.19 to 0.70)	0.210	-0.90 (-2.50 to 0.70)	0.271
Group×T3	-0.15 (-1.82 to 1.52)	0.861	-0.15 (-0.77 to 0.46)	0.627	-0.33 (-2.51 to 1.84)	0.763	0.41 (-1.25 to 2.07)	0.625

Abbreviations: BMI=body mass index, CESEI=Cardiac Exercise Self-Efficacy Instrument, CLASP=Cardiovascular Limitations and Symptoms Profile, CRP=C-reactive protein, DBP=diastolic blood pressure, EQ5-D VAS=EuroQol five dimensions questionnaire visual analogue scale, HDL=high-density lipoprotein, ISWT=incremental shuttle walk test, LDL=low-density lipoprotein, MET=metabolic equivalent of task, SBP=systolic blood pressure, TC=total cholesterol

TABLE 2. (cont'd)

Variable	Regression coefficient (95% confidence interval)	P value	Regression coefficient (95% confidence interval)	P value	Regression coefficient (95% confidence interval)	P value	Regression coefficient (95% confidence interval)	P value
	10-m ISWT		CESEI total score		CLASP		EQ5-D VAS	
	SBP		DBP		Pulse rate		Haemoglobin A1c	
Group	-3.55 (-8.48 to 1.37)	0.157	-1.79 (-5.07 to 1.50)	0.287	0.40 (-3.72 to 4.52)	0.849	-0.09 (-0.36 to 0.18)	0.524
T1	4.67 (-0.32 to 9.65)	0.066	0.88 (-1.63 to 3.39)	0.493	-0.88 (-4.23 to 2.48)	0.608	-0.03 (-0.12 to 0.07)	0.592
T2	7.64 (2.83 to 12.45)	0.002	0.67 (-1.72 to 3.07)	0.582	-2.40 (-5.02 to 0.22)	0.073	0.07 (-0.02 to 0.16)	0.140
T3	3.58 (-2.08 to 9.24)	0.215	-1.44 (-3.68 to 0.80)	0.207	-1.20 (-4.49 to 2.09)	0.475	0.09 (-0.02 to 0.20)	0.117
Group×T1	-0.52 (-6.86 to 5.82)	0.872	-0.88 (-4.35 to 2.59)	0.619	-0.70 (-5.16 to 3.77)	0.760	0.13 (-0.02 to 0.27)	0.086
Group×T2	-1.21 (-8.17 to 5.75)	0.734	-0.16 (-3.50 to 3.18)	0.925	-0.82 (-4.75 to 3.12)	0.685	0.04 (-0.13 to 0.21)	0.639
Group×T3	0.10 (-7.05 to 7.24)	0.979	1.87 (-1.33 to 5.07)	0.251	-1.12 (-5.59 to 3.36)	0.624	0.06 (-0.12 to 0.25)	0.498
	Fasting blood glucose		Total cholesterol		HDL-cholesterol		TC to HDL-cholesterol ratio	
Group	-0.46 (-0.94 to 0.03)	0.066	0.05 (-0.23 to 0.32)	0.743	0.01 (-0.08 to 0.11)	0.771	0.04 (-0.26 to 0.33)	0.815
T1	-0.14 (-0.39 to 0.11)	0.277	-0.05 (-0.23 to 0.14)	0.616	0.00 (-0.03 to 0.04)	0.887	0.03 (-0.22 to 0.27)	0.838
T2	0.13 (-0.07 to 0.33)	0.196	-0.09 (-0.22 to 0.04)	0.167	0.00 (-0.04 to 0.05)	0.925	-0.06 (-0.18 to 0.06)	0.328
T3	0.22 (-0.08 to 0.52)	0.156	0.04 (-0.12 to 0.20)	0.616	0.03 (-0.02 to 0.07)	0.307	-0.05 (-0.21 to 0.11)	0.548
Group×T1	0.15 (-0.17 to 0.47)	0.354	0.09 (-0.14 to 0.31)	0.451	0.02 (-0.04 to 0.07)	0.619	-0.06 (-0.35 to 0.22)	0.660
Group×T2	-0.09 (-0.40 to 0.21)	0.548	0.12 (-0.09 to 0.33)	0.248	0.05 (-0.02 to 0.12)	0.155	-0.04 (-0.26 to 0.17)	0.684
Group×T3	0.09 (-0.32 to 0.50)	0.665	0.02 (-0.21 to 0.25)	0.844	0.04 (-0.02 to 0.11)	0.193	-0.13 (-0.36 to 0.11)	0.288
	LDL-cholesterol		Triglyceride		High-sensitivity CRP			
Group	0.05 (-0.19 to 0.30)	0.663	0.00 (-0.25 to 0.25)	0.994	0.20 (-0.21 to 0.61)	0.340		
T1	-0.09 (-0.25 to 0.08)	0.317	0.09 (-0.09 to 0.26)	0.336	-0.19 (-0.53 to 0.15)	0.265		
T2	-0.08 (-0.19 to 0.02)	0.113	-0.01 (-0.16 to 0.14)	0.889	-0.19 (-0.49 to 0.11)	0.210		
T3	0.01 (-0.12 to 0.14)	0.881	0.02 (-0.18 to 0.22)	0.839	-0.22 (-0.51 to 0.06)	0.129		
Group×T1	0.11 (-0.09 to 0.31)	0.270	-0.13 (-0.35 to 0.08)	0.227	-0.02 (-0.46 to 0.42)	0.923		
Group×T2	0.09 (-0.10 to 0.27)	0.361	-0.07 (-0.31 to 0.17)	0.552	0.02 (-0.40 to 0.44)	0.925		
Group×T3	0.02 (-0.19 to 0.22)	0.874	-0.12 (-0.40 to 0.16)	0.388	0.01 (-0.39 to 0.41)	0.963		
Regression coefficient	Lightly active activity		Fairly active activity		Very active activity		Total activity	
Group	0.61 (-1.00 to 2.22)	0.459	0.57 (-0.19 to 1.33)	0.140	0.73 (-0.16 to 1.61)	0.110	1.03 (-0.80 to 2.86)	0.270
T1	-0.02 (-1.94 to 1.90)	0.983	-0.17 (-0.97 to 0.63)	0.680	-0.42 (-1.45 to 0.60)	0.419	-0.19 (-2.42 to 2.03)	0.867
T2	1.28 (-0.10 to 2.67)	0.069	0.42 (-0.06 to 0.89)	0.084	0.68 (-0.03 to 1.39)	0.059	1.55 (0.05 to 3.05)	0.043
T3	-0.64 (-2.34 to 1.06)	0.460	-0.02 (-0.74 to 0.71)	0.969	0.13 (-0.81 to 1.07)	0.780	-0.49 (-2.45 to 1.47)	0.621
Group×T1	0.71 (-1.71 to 3.13)	0.566	0.24 (-0.79 to 1.27)	0.652	0.08 (-1.16 to 1.32)	0.900	0.71 (-2.03 to 3.45)	0.613
Group×T2	0.06 (-2.04 to 2.15)	0.959	0.24 (-0.88 to 1.36)	0.671	-0.84 (-1.92 to 0.24)	0.126	-0.12 (-2.47 to 2.23)	0.920
Group×T3	0.18 (-2.13 to 2.48)	0.881	-0.47 (-1.43 to 0.50)	0.342	-1.09 (-2.28 to 0.10)	0.073	-0.45 (-3.05 to 2.14)	0.732

The bootstrapping method was used to estimate 95% CIs for incremental effects. The bootstrapped 10 000 pairs of incremental costs and incremental effects were plotted on a cost-effectiveness curve to illustrate uncertainty surrounding the cost-effectiveness ratio. All statistical tests were two-sided, and the significance level was set at 0.05.

Results

Among 348 patients with CHD, 130 agreed to participate. The mean age of participants was 64.24 years. The intervention and control groups were comparable in terms of demographics (Table 1).

Compared with the control group, the intervention group demonstrated significantly greater improvements in exercise capacity at T1 (P=0.034) and in exercise self-efficacy at T2 (P=0.043) and T3 (P=0.015) [Table 2].

The mean overall QALY levels over 15 months were 1.2295 in the intervention group and 1.2262 in the control group. MPPA intervention led to a

greater gain of 0.0033 (95% bootstrap CI= -0.0096 to 0.0164) QALYs and a higher total cost of HK$198 (95% bootstrap CI=71.5 to 338.3), compared with the control group. The mean cost per patient for 1 QALY gain by MPPA intervention was HK$60 182 (~US$7716), which was <3 times the gross domestic product per capita (US$ 49 660.6 in 2021). Thus, the MPPA intervention was considered cost-effective. The cost-effectiveness curve shows the ICERs of the bootstrapped results with 10 000 replications; 69% of the bootstrapped cost-effectiveness data indicated that the MPPA intervention was considerably more effective but more expensive than the usual care in terms of QALY improvement.

Discussion

MPPA can be an effective strategy to enhance exercise capacity for 3 months and exercise self-efficacy for 15 months. The lack of a long-term effect on exercise capacity may be attributed to the COVID-19 pandemic and corresponding infection control measures. Although the patients' indoor activities may not have been restricted, the reduced outdoor activity and negative behavioural changes could have led to a decrease in total PA time.[7]

There was no significant effect of MPPA intervention on PA level, compared with the usual care. However, the intervention group showed a greater improvement in accelerometer-measured PA level at T1, compared with the control group. This may have contributed to the significantly improved exercise capacity in the intervention group at 3 months. The lack of a significant effect on exercise capacity at 15 months may have been attributed to social restrictions during the pandemic and the high PA level that already contributed to great benefits.

There was no significant difference between groups regarding clinical parameters. Clinical outcomes are affected by many aspects other than exercise such as lifestyle modifications. Therefore, comprehensive CR programmes should focus on modifying cardiovascular risk factors and unhealthy lifestyles.

Compared with the control group, the intervention group did not exhibit significant effects on HRQoL. Nevertheless, in addition to changes observed in the control group, the intervention group displayed improvements in HRQoL at T1 and T2. There was no significant difference between groups regarding self-determination. Nevertheless, a trend toward improvement was present in both groups.

Conclusion

The combination of music with exercise training may enhance short-term exercise capacity and long-term exercise self-efficacy. The MPPA intervention is more effective but more expensive than the usual care for improving QALYs. There was no significant difference between groups regarding other outcomes; most outcomes showed a trend toward improvement.

Funding

This study was supported by the Health and Medical Research Fund, Health Bureau, Hong Kong SAR Government (#14152621). The full report is available from the Health and Medical Research Fund website (https://rfs2.healthbureau.gov.hk).

Disclosure

The results of this research have been previously published in:

1. Chair SY, Leung KC, Lo SWZ, et al. Exercise capacity and its determinants among postcardiac rehabilitation patients with coronary heart disease. Nurs Open 2023;10:2501-7.
2. Chair SY, Cheng HY, Lo SWS, et al. Effectiveness of a home-based music-paced physical activity programme on exercise-related outcomes after cardiac rehabilitation: a randomized controlled trial. Eur J Cardiovasc Nurs 2024:zvad115.

References

1. Terry PC, Karageorghis CI, Curran ML, Martin OV, Parsons-Smith RL. Effects of music in exercise and sport: a meta-analytic review. Psychol Bull 2020;146:91-117.
2. Chair SY, Zou H, Cao X. A systematic review of effects of recorded music listening during exercise on physical activity adherence and health outcomes in patients with coronary heart disease. Ann Phys Rehabil Med 2021:64:101447.
3. DiMatteo MR, DiNicola DD. Achieving Patient Compliance: the Psychology of the Medical Practitioner's Role. Pergamon; 1982.
4. Deci EL, Ryan RM. Self-determination theory. In: van Lange PAM, Kruglanski AW, Higgins ET, editors. Handbook of Theories of Social Psychology. Sage Publications; 2012: 416-36.
5. World Bank. World Bank national accounts data, and OECD National Accounts data files. GDP per capita (current US$) – Hong Kong SAR, China. Accessed 19 September 2022. Available from: https://data.worldbank.org/indicator/NY.GDP.PCAP.CD?locations=HK
6. Marseille E, Larson B, Kazi DS, Kahn JG, Rosen S. Thresholds for the cost-effectiveness of interventions: alternative approaches. Bull World Health Organ 2015;93:118-24.
7. Yamada M, Kimura Y, Ishiyama D, et al. The influence of the COVID-19 pandemic on physical activity and new incidence of frailty among initially non-frail older adults in Japan: a follow-up online survey. J Nutr Health Aging 2021;25:751-6.

Client Service Receipt Inventory for rare genetic diseases in Hong Kong: abridged secondary publication

CCY Chung, WHS Wong, SL Lee, BHY Chung *

KEY MESSAGES

1. The Client Service Receipt Inventory for the rare genetic disease population in Hong Kong (CSRI-Ra) was validated to capture both direct and indirect costs of rare diseases from a societal perspective.
2. Pilot testing of the CSRI-Ra demonstrated moderate to good agreement between utilisation records and electronic patient records, indicating that criterion (concurrent) validity was acceptable.
3. The CSRI-Ra, alone or in combination with electronic patient records, is valid for health- and social-care planning.

Hong Kong Med J 2024;30(Suppl 1):S23-6
HMRF project number: 07182426

CCY Chung, WHS Wong, SL Lee, BHY Chung

Department of Paediatrics and Adolescent Medicine, School of Clinical Medicine, LKS Faculty of Medicine, The University of Hong Kong, Hong Kong SAR, China

* Principal applicant and corresponding author: bhychung@hku.hk

Introduction

Genomic medicine increases public awareness of rare diseases (RDs). In Hong Kong, one in 67 people is living with one or more RDs.[1] RDs have broad health- and social-care implications that extend beyond the public health system perspective with regard to effective health- and social-care planning.

The direct costs of RDs include healthcare expenditures; indirect costs include reduced productivity and lost opportunities. There is a lack of standardised tools to collect indirect cost-related data, hindering assessment of the true burden of RDs. In Hong Kong, no tool is available to capture service utilisation data outside of the Hospital Authority. The Client Service Receipt Inventory (CSRI) is a common resource-use measurement tool that evaluates service utilisation patterns to estimate associated costs across healthcare, social care, and community settings. It is a reliable and valid tool for the collection of data related to socio-economic costs.[2-4] The development and adaption of the CSRI in the RD population for the first time in any jurisdiction and language would allow a comprehensive assessment of RD's implications, providing meaningful results to both clinicians and healthcare policy makers. Acknowledging the need for the development of a resource-use measurement tool in Hong Kong, the current study sought to develop, contextualise, translate, and validate the CSRI for the RD population in Hong Kong (CSRI-Ra).

Methods

The CSRI-Ra was developed through focus group meetings, in-depth interviews, and data analysis using a thematic framework. Focus group participants included patients with RDs, family members/caregivers of patients, health professionals, and staff from non-governmental organisations (NGOs) and special schools. Two focus group meetings were conducted in August 2019. The first meeting included patients with RDs and family members/caregivers of patients to collect data specific to the RD population. The second meeting included professionals from health- and social-care settings to collect data concerning the accessibility and availability of services and resources. The meetings were conducted in Cantonese and audio- and video-recorded. Collected data were grouped into emerging semantic themes and analysed using a combined inductive and deductive identification approach.[5] Discrepancies were identified and resolved.

Previous CSRIs were used to guide the structure of the CSRI-Ra. All identified themes, subthemes, and variables were grouped into five sections: background information, household and caregiver support, healthcare service and resource utilisation, community support, and education and employment. An expert panel discussion was conducted to ensure that the CSRI-Ra was sufficiently standardised but sensitive to the local context.

The CSRI-Ra was forward-translated to traditional Chinese and backward-translated to English by four independent bilingual researchers. Discrepancies were identified and resolved.

To achieve face validity and semantic equivalence, the content and language of both Chinese and English versions were addressed among

focus group participants through telephone and email discussions. Face-to-face interviews with three additional allied health workers were conducted to ensure that both versions were sufficiently adapted to the Hong Kong setting. Ten bilingual university students were randomly selected to provide suggestions for improvement as the general public. Both versions were validated among eight bilingual patients with RDs and caregivers of patients to assess their alternate-form reliability using intra-class correlation coefficients (ICCs), along with two-way random-effects models based on single ratings and absolute agreement.

The criterion validity of the CSRI-Ra was assessed in a pilot cohort comprising 94 independent patients with RDs and caregivers of patients. Agreement between the self-/proxy-reported utilisation record collected from the CSRI-Ra and the actual utilisation record in the electronic patient record (ePR) was assessed using ICCs with two-way random-effects models. The numbers of accident and emergency (A&E), inpatient, and outpatient visits were compared.

Results

In the first focus group, there were eight participants covering six RDs with heterogeneity in terms of disability type, treatment needs, and service and resource availability (Table 1). The expert panel considered these six RDs to be sufficiently representative of the RD population in Hong Kong. Additionally, the nine participants in the second focus group had a mean of 12 years of experience related to RDs (Table 2).

Data were analysed using thematic analysis and grouped into the five sections. Two versions were developed: self-completed (patient version) and proxy-completed (caregiver version).

Agreement between the English and Chinese versions of the CSRI-Ra was assessed in eight bilingual participants (two patients with RDs and six caregivers of patients), with a mean of 51.4 days between completion of the two versions. The overall ICC was 0.91 (95% confidence interval [CI]=0.89-0.92), which indicated excellent agreement between the two versions. The ICCs were 0.89 (95% CI=0.86-0.92) for the self-completed version and 0.93 (95% CI=0.91-0.95) for the proxy-completed version.

Agreement between the CSRI-Ra and the ePR was assessed in 94 participants (Table 3). Among them, 54 (57.4%) completed the patient version and 40 (42.6%) completed the caregiver version. In total, 45 RDs were recorded. The overall ICC between the self-/proxy-completed CSRI-Ra and the ePR was 0.69 (95% CI=0.56-0.78), which indicated moderate to good agreement and acceptable criterion (concurrent) validity. Both the patient version (ICC=0.67, 95% CI=0.50-0.80) and the caregiver version (ICC=0.70, 95% CI=0.50-0.80) demonstrated moderate to good agreement. Subgroup analyses of item performance based on the numbers of A&E, inpatient, and outpatient visits revealed acceptable convergent and discriminant validities. Agreement was highest for inpatient services (ICC=0.81, 95% CI=0.73-0.87).

TABLE 1. Characteristics of participants in the first focus group meeting (n=8)

Characteristics	No. (%) of participants
Role	
Patient with rare disease (RD)	2 (25.0)
Family member/informal caregiver of patient with RD	6 (75.0)
Sex	
Female	5 (62.5)
Male	3 (37.5)
Age group, y	
18-25	0
26-30	1 (12.5)
31-35	0
36-40	2 (25.0)
41-45	1 (12.5)
>45	4 (50.0)
Education level	
Primary or below	0
Secondary	0
Post-secondary/associate's degree or equivalent	1 (12.5)
Bachelor's degree	2 (25.0)
Master's/doctoral degree	5 (62.5)
RD	
Achondroplasia	1 (12.5)
Marfan syndrome	2 (25.0)
Mucopolysaccharidosis type 6	2 (25.0)
Pompe disease	1 (12.5)
Tuberous sclerosis	1 (12.5)
Williams syndrome	1 (12.5)
Experience completing research questionnaires	
Questionnaires related to RDs	6 (75.0)
Questionnaires related to service use/resource use	2 (25.0)

Discussion

The CSRI-Ra, available at https://paed.hku.hk/e-form/csri-ra-registration-form.asp, is validated for use in the RD population in Hong Kong. It is a standardised tool to measure RD costs from a

societal perspective.

The burden of RDs in Hong Kong has been assessed from a health system perspective. In 2015-16, the inpatient cost of RDs was estimated to be HK$1 594 339 530, corresponding to 4.3% of total inpatient costs for the Hospital Authority.[1] However, the true burden of RDs has not been estimated. The CSRI-Ra enables quantification of the socio-economic burden of RDs, along with informed health- and social-care planning.

The CSRI-Ra relies on participant recall for data collection. The validation stage demonstrated that the CSRI-Ra had acceptable criterion (concurrent) validity, indicating that the collected data are comparable with the ePR. The reliability and validity of CSRIs in other health areas have been demonstrated.[2-4] The CSRI-Ra offers both self-completed and proxy-completed versions, allowing data collection across a wide range of patients with various ages and disease severities. The CSRI-Ra considers the uniqueness of RDs and can be generalised to other contexts and populations, allowing international comparisons of RD burden.

There were some limitations in this study. Despite its acceptable criterion validity, the present study only compared the number of A&E, outpatient, and inpatient visits between CSRI-Ra and ePR. We did not assess hospital and community services in private settings; nor did we explore caregiver support or employment situations; the corresponding datasets were inaccessible or unavailable in ePR and existing databases. Nonetheless, the acceptable agreement between the CSRI-Ra and the ePR reflects the reliability of the tool and suggests its application in areas beyond the health system perspective for the estimation of socio-economic burden related to RDs.

Conclusion

The CSRI-Ra enables estimation of economic impacts from a societal perspective and better understanding of RD-related service and resource utilisation patterns in Hong Kong, thereby informing health- and social-care planning.

Funding

This study was supported by the Health and Medical Research Fund, Health Bureau, Hong Kong SAR Government (#07182426). The full report is available from the Health and Medical Research Fund website (https://rfs2.healthbureau.gov.hk).

Disclosure

The results of this research have been previously published in:

TABLE 2. Characteristics of participants in the second focus group meeting (n=9)

Characteristics	Value*
Role	
Nurse (based in special school)	1 (11.1)
Social worker	2 (22.2)
Special school principal/teacher	3 (33.3)
Manager/coordinator/staff in non-governmental organisation	3 (33.3)
Sex	
Female	7 (77.8)
Male	2 (22.2)
Age group, y	
18-25	0
26-30	2 (22.2)
31-35	0
36-40	3 (33.3)
41-45	1 (11.1)
>45	3 (33.3)
Education level	
Primary or below	0
Secondary	0
Post-secondary/associate's degree or equivalent	2 (22.2)
Bachelor's degree	3 (33.3)
Master's/doctoral degree	4 (44.4)
Experience related to rare diseases, y	12.0±6.8
<5	0
5-9	4 (44.4)
10-14	2 (22.2)
15-19	1 (11.1)
≥20	2 (22.2)
Target patient type	
Physical disability	6 (66.7)
Intellectual disability	9 (100.0)
Psychological/mental problems	3 (33.3)
Visual impairment	6 (66.7)
Hearing impairment	5 (55.6)
Others	1 (11.1)
Target patient age group	
Infants (<1 y)	1 (11.1)
Toddlers (1-2 y)	1 (11.1)
Children (3-12 y)	5 (55.6)
Adolescents (13-18 y)	6 (66.7)
Adults (>18 y)	5 (55.6)
Older adults (≥65 y)	3 (33.3)
Experience completing research questionnaires	
Questionnaires related to rare diseases	0
Questionnaires related to service use/resource use	0

* Data are presented as mean±standard deviation or No. (%) of participants

TABLE 3. Agreement between the Client Service Receipt Inventory for rare genetic disease population in Hong Kong and the electronic patient record

	Intra-class correlation coefficient (95% confidence interval)		
	Overall	Self-completed (patient version)	Proxy-completed (caregiver version)
Overall service utilisation	0.69 (0.56-0.78)	0.67 (0.50-0.80)	0.70 (0.50-0.83)
Inpatient visits	0.81 (0.73-0.87)	0.81 (0.70-0.89)	0.79 (0.64-0.89)
Outpatient visits	0.60 (0.45-0.71)	0.46 (0.22-0.65)	0.67 (0.46-0.81)
Accident and emergency visits	0.58 (0.42-0.70)	0.66 (0.48-0.79)	0.33 (0.03-0.58)

1. Chung CCY, Fung JLF, Lui ACY, et al. Client Service Receipt Inventory as a standardised tool for measurement of socio-economic costs in the rare genetic disease population (CSRI-Ra). Sci Rep 2021;11:23837.

Acknowledgements

We thank all patients, caregivers, and health- and social-care professionals for participation, as well as Rare Disease Hong Kong, Duchess of Kent Children's Hospital, Queen Mary Hospital, and all special schools and non-governmental organisations that participated in recruitment. We acknowledge Prof Martin Knapp and Dr Eva Bonin from the Care Policy and Evaluation Centre at the London School of Economics and Political Science for providing valuable advice and support.

References

1. Chiu ATG, Chung CCY, Wong WHS, Lee SL, Chung BHY. Healthcare burden of rare diseases in Hong Kong - adopting ORPHAcodes in ICD-10 based healthcare administrative datasets. Orphanet J Rare Dis 2018;13:147.
2. Byford S, Leese M, Knapp M, et al. Comparison of alternative methods of collection of service use data for the economic evaluation of health care interventions. Health Econ 2007;16:531-6.
3. Heinrich S, Deister A, Birker T, et al. Accuracy of self-reports of mental health care utilization and calculated costs compared to hospital records. Psychiatry Res 2011;185:261-8.
4. Patel A, Rendu A, Moran P, Leese M, Mann A, Knapp M. A comparison of two methods of collecting economic data in primary care. Fam Pract 2005;22:323-7.
5. Nowell LS, Norris JM, White DE, Moules NJ. Thematic analysis: striving to meet the trustworthiness criteria. Int J Qual Methods 2017;16.

Radiosensitivity index as a predictive biomarker for radiotherapy de-intensification in nasopharyngeal carcinoma: abridged secondary publication

CL Chiang *, WMA Lee, CWH Choi, KCR Ngan, WT Ng, HFV Lee, TC Lam, KO Lam, KC Tsang, WHJ Wong

KEY MESSAGES

1. The radiosensitivity index is a potential predictor for locoregional control in radiotherapy-treated patients with locally advanced nasopharyngeal cancer.
2. Owing to the small sample size, the association between radiosensitivity index and late toxicity is inconclusive.

Hong Kong Med J 2024;30(Suppl 1):S27-8
HMRF project number: 06172046

[1] CL Chiang, [1] WMA Lee, [2] CWH Choi, [2] KCR Ngan, [1] WT Ng, [1] HFV Lee, [1] TC Lam, [1] KO Lam, [1] KC Tsang, [3] WHJ Wong

[1] *Department of Clinical Oncology, School of Clinical Medicine, LKS Faculty of Medicine, The University of Hong Kong, Hong Kong SAR, China*
[2] *Division of Epidemiology and Biostatistics, School of Public Health, LKS Faculty of Medicine, The University of Hong Kong, Hong Kong SAR, China*
[3] *School of Biomedical Science, LKS Faculty of Medicine, The University of Hong Kong, Hong Kong SAR, China*

* Principal applicant and corresponding author: chiangcl@hku.hk

Introduction

In 2018, nasopharyngeal carcinoma (NPC) affected more than 70 000 individuals worldwide. Radiotherapy (RT) is the primary treatment for NPC; patients with the same tumour, node, and metastasis stage receive similar doses of RT based on a stage-based strategy.[1]

Improvements in anatomic precision can increase tumour control and decrease complications. Intensity-modulated RT improves the 5-year locoregional control rate to approximately 90%, even in patients with locally advanced NPC. However, treatment for NPC continues to use the stage-based strategy, whereby tumours with similar anatomic extent receive identical doses of radiation. This one-size-fits-all approach fails to address the biological heterogeneity of cancer.

Moffitt Cancer Center has developed a gene expression-based radiosensitivity index (RSI),[1] which was validated as an independent predictor for clinical outcomes in RT-treated patients. The genomic-guided radiation dose model integrates the gene expression-based RSI with a linear quadratic model of radiation prescription to establish a precision medicine framework for radiation oncology.[2] Personalised RT for patients with NPC also addresses tissue-related complications. The Radiogenomics Consortium considers radiation toxicity to be genetically predetermined. The radiosensitivity pathway in NPC is used to predict tumour control and late toxicity incidence.[3] We hypothesised that the RSI can serve as a predictive biomarker for tumour control, survival, and late toxicity. We aimed to evaluate the predictive value of the RSI in RT-treated patients with locally advanced NPC.[4]

Methods

We analysed archived specimens from the NPC-0501 trial.[4] In total, 803 patients with locally advanced NPC (stage III to IVb) were recruited between September 2006 and September 2012. Pre-treatment formalin-fixed, paraffin-embedded tissue samples were available from 243 patients; 71 samples were excluded owing to inadequate tumour cells. Therefore, 172 samples were reviewed, but 80 of the samples demonstrated poor quality. The remaining 92 samples were analysed using the RSI model.

Results

Of the 92 patients with NPC included, 74 were classified as radiosensitive (RS) and 18 were classified as radioresistant (RR). The two groups were comparable in terms of demographics.

At the median follow-up interval of 7.1 (range, 0.8-11.9) years, 27 patients had died of disease progression (n=26) or brain abscess (n=1). RS patients had higher rates than RR patients in terms of the 3-year and 5-year locoregional failure-free rates (84.4% vs 64.9% and 84.4% vs 51.4%, respectively; P=0.001, adjusted P=0.009) as well as the 3-year and 5-year overall survival rates.

Of the 92 patients, 20 developed severe (≥grade 3) late toxicity: peripheral neuropathy (n=9, 9.8%), ear-related (deafness/otitis) [n=9, 9.8%], and soft tissue/bone damage (n=3, 3.3%). The RS and RR patients were comparable in terms of the incidence of late toxicity (P=0.491) and serious late toxicity-free rate (P=0.532).

Discussion

NPC is radiosensitive; we identified genomically distinct patient populations who experienced differential benefits from radiation. The RSI is an independent predictor for survival outcomes among RT-treated patients with NPC, consistent with reports that the RSI is an assay of radiosensitivity independent of disease sites. Our genomic-guided radiation dose model provides a framework for adjusting RT doses among patients with NPC according to individual tumour radiosensitivity.

The use of a biomarker-based model to guide RT prescription may improve treatment outcomes. The RSI has been biologically and clinically validated. Use of the RSI may avoid multiple tests, and use of a pre-defined cut-off may avoid potential bias. All patients included were participants in a phase III multicentre randomised controlled trial (NPC-0501 study); the tissue specimens were prospectively collected. The clinical validity of the RSI is supported by level I scientific evidence.

The RSI is an independent predictor for locoregional control in RT-treated patients with locally advanced NPC. Patients with primary NPC received uniformly high-dose radiation (66-76 Gy); the dose of RT may have eliminated differences in tumour radiosensitivity; only high RR tumours will develop local recurrence. However, patients harbouring microscopic disease usually receive a modest dose of radiation (50-60 Gy); radiosensitivity becomes relevant because larger numbers of such patients receive insufficient radiation doses.

There was no correlation between the RSI and the incidence of late toxicity, contrary to our hypothesis that radiosensitivity of tumour and normal tissue is related. Candidate gene studies and genome-wide association studies are needed to identify biomarkers that can predict normal tissue toxicity.

The present study had several limitations. The sample size was small. Patients were randomised into six treatment arms, which may have affected clinical outcomes. Data were obtained from an endemic region where the main NPC subtype is undifferentiated non-keratinising carcinoma. All included patients had locally advanced NPC tumours (T3/4 or N0-3) and were treated with concurrent chemotherapy plus (neo)adjuvant chemotherapy.

Conclusion

The RSI is an independent predictor for survival outcomes, but not toxicity, among RT-treated patients with NPC.

Funding

This study was supported by the Health and Medical Research Fund, Health Bureau, Hong Kong SAR Government (#06172046). The full report is available from the Health and Medical Research Fund website (https://rfs2.healthbureau.gov.hk).

References

1. Lee AW, Ma BB, Ng WT, Chan AT. Management of nasopharyngeal carcinoma: current practice and future perspective. J Clin Oncol 2015;33:3356-64.
2. Scott JG, Berglund A, Schell MJ, et al. A genome-based model for adjusting radiotherapy dose (GARD): a retrospective, cohort-based study. Lancet Oncol 2017;18:202-11.
3. Chua K, Ahamed W, Shwe TT, et al. Lymphocyte apoptosis as a predictive biomarker for radiation therapy de-intensification in EBV-associated nasopharynx cancer. Int J Radiat Oncol Biol Phys 2017;99:S123.
4. Lee AWM, Ngan RKC, Ng WT, et al. NPC-0501 trial on the value of changing chemoradiotherapy sequence, replacing 5-fluorouracil with capecitabine, and altering fractionation for patients with advanced nasopharyngeal carcinoma. Cancer 2020;126:3674-88.

Genome-wide DNA methylation profiling for central nervous system embryonal tumours in children: abridged secondary publication

APY Liu *, GCF Chan, BHY Chung, W Yang, HK Ng

KEY MESSAGES

1. Genome-wide DNA methylation profiling enables tumour classification of central nervous system (CNS) tumour tissues.
2. Methylation profiling demonstrates utility in the diagnostic process of CNS embryonal tumours, facilitating tumour subgrouping in two-thirds of patients while allowing consideration of alternative diagnoses in one-tenth of patients.
3. Epigenome-based classification of CNS embryonal tumours stratified patients into prognostically relevant disease subgroups.

Hong Kong Med J 2024;30(Suppl 1):S29-33
HMRF project number: 06171666

[1,2] **APY Liu**, [1,2] **GCF Chan**, [1] **BHY Chung**, [1] **W Yang**, [3] **HK Ng**

[1] *Department of Paediatrics and Adolescent Medicine, School of Clinical Medicine, Li Ka Shing Faculty of Medicine, The University of Hong Kong, Hong Kong SAR, China*
[2] *Department of Paediatrics and Adolescent Medicine, Hong Kong Children's Hospital, Hong Kong SAR, China*
[3] *Department of Anatomical and Cellular Pathology, The Chinese University of Hong Kong, Hong Kong SAR, China*

* Principal applicant and corresponding author: apyliu@hku.hk

Introduction

Central nervous system (CNS) tumours are the most common solid tumours in children, with the highest mortality among various paediatric malignancies.[1] In particular, CNS embryonal tumours are associated with poor survival despite the availability of multi-modal treatment with maximal surgical resection, radiation therapy, and chemotherapy. In addition, survivors of such conditions often experience long-term treatment-related toxicity, which negatively impacts their quality of life. The difficulty managing paediatric CNS embryonal tumours is partly related to their molecular heterogeneity. Advances in high-throughput genomic techniques, specifically DNA methylation arrays, have revealed important molecular subgroups within histologically defined entities. CNS embryonal tumours and associated high-grade neuroepithelial tumours (HGNETs), including medulloblastoma, CNS-primitive neuroectodermal tumour (PNET), atypical teratoid/rhabdoid tumour (ATRT), and pineoblastoma, have been classified as clinically relevant epigenomic subgroups.[2] Such molecular classifications have been incorporated into iterations of the World Health Organization (WHO) CNS Tumour Classification.

DNA methylation arrays are increasingly utilised to aid clinical diagnosis, treatment decision, and study trial design. However, their clinical value is dependent on pre-existing diagnostic infrastructure and expertise. We successfully profiled archival tumour tissue from a cohort of paediatric CNS embryonal tumours and HGNETs. We demonstrated the utility DNA methylation arrays in diagnostics and outcome prediction.

Methods

Prior to 2019, paediatric patients with cancer in Hong Kong were managed in one of the five paediatric oncology units of the Hong Kong Paediatric Haematology/Oncology Study Group. We retrospectively identified patients with CNS embryonal tumours and associated diagnostic entities who were treated between 1999 and 2017. The relevant histologic entities included medulloblastoma, CNS-PNET, pineal parenchymal tumour, embryonal tumours with multi-layered rosettes (ETMR), embryonal tumour not otherwise specified, and HGNET. Patients with adequate archival tumour tissue were included.

Formalin-fixed paraffin-embedded (FFPE) tumour samples were retrieved, and DNA extraction was performed. Extracted DNA was quantified, and quality control was performed. DNA samples that met the quality control criteria (delta-Ct <5) underwent bisulphite conversion and were subsequently used for DNA methylation profiling targeting 850 000 CpG sites in the genome. The resulting raw Intensity Data files were analysed with the web-based DKFZ classifier (Molecular Neuropathology [MNP] 2.0 v11b4 https://www.molecularneuropathology.org/mnp), where each sample was assigned a molecular class and corresponding confidence score (Fig 1). In parallel, unsupervised t-distributed stochastic neighbour embedding (t-SNE) analysis was performed to compare tumours in this study with a publicly available CNS tumour reference cohort comprising 2801 samples.[3] Molecular classes were based on the results of both analyses and interpreted according to clinical context.

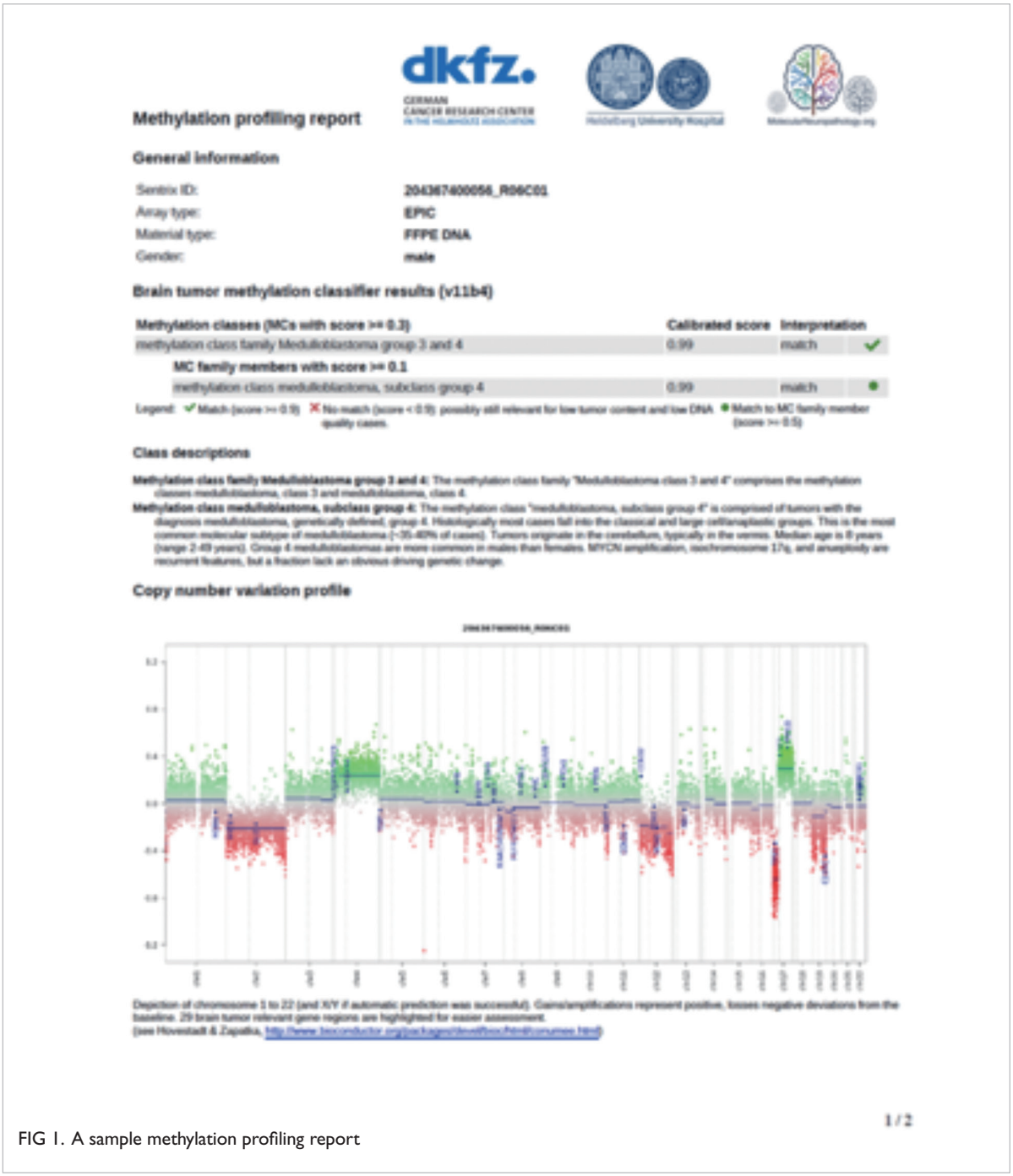

Methylation profiling report

General information

Sentrix ID:	204367400056_R06C01
Array type:	EPIC
Material type:	FFPE DNA
Gender:	male

Brain tumor methylation classifier results (v11b4)

Methylation classes (MCs with score >= 0.3)	Calibrated score	Interpretation
methylation class family Medulloblastoma group 3 and 4	0.99	match
MC family members with score >= 0.1		
methylation class medulloblastoma, subclass group 4	0.99	match

Legend: Match (score >= 0.9) No match (score < 0.9): possibly still relevant for low tumor content and low DNA quality cases. Match to MC family member (score >= 0.5)

Class descriptions

Methylation class family Medulloblastoma group 3 and 4: The methylation class family "Medulloblastoma class 3 and 4" comprises the methylation classes medulloblastoma, class 3 and medulloblastoma, class 4.

Methylation class medulloblastoma, subclass group 4: The methylation class "medulloblastoma, subclass group 4" is comprised of tumors with the diagnosis medulloblastoma, genetically defined, group 4. Histologically most cases fall into the classical and large cell/anaplastic groups. This is the most common molecular subtype of medulloblastoma (~35-40% of cases). Tumors originate in the cerebellum, typically in the vermis. Median age is 8 years (range 2-49 years). Group 4 medulloblastomas are more common in males than females. MYCN amplification, isochromosome 17q, and aneuploidy are recurrent features, but a fraction lack an obvious driving genetic change.

Copy number variation profile

Depiction of chromosome 1 to 22 (and X/Y if automatic prediction was successful). Gains/amplifications represent positive, losses negative deviations from the baseline. 29 brain tumor relevant gene regions are highlighted for easier assessment.
(see Hovestadt & Zapatka, http://www.bioconductor.org/packages/devel/bioc/html/conumee.html)

1 / 2

FIG 1. A sample methylation profiling report

Overall survival was defined as the interval from diagnosis to date of death or final follow-up for survivors; progression-free survival was defined as the interval from the date of diagnosis to the date of the first event (disease progression, disease recurrence, second malignant neoplasm, or death from any cause) or final follow-up for patients without events. Survival estimates were reported using the Kaplan-Meier method. The log-rank test was used to compare outcomes among groups, and Cox regression was used for multivariate analysis. All P values were two-sided and considered statistically significant at <0.05.

Results

In total, 124 FFPE tumour samples were profiled by methylation arrays. Among these samples, 97 contained histologic CNS embryonal tumours/HGNETs, 16 contained histologic glioneuronal tumours that served as comparative controls, and 11 required repeat analysis due to technical issues

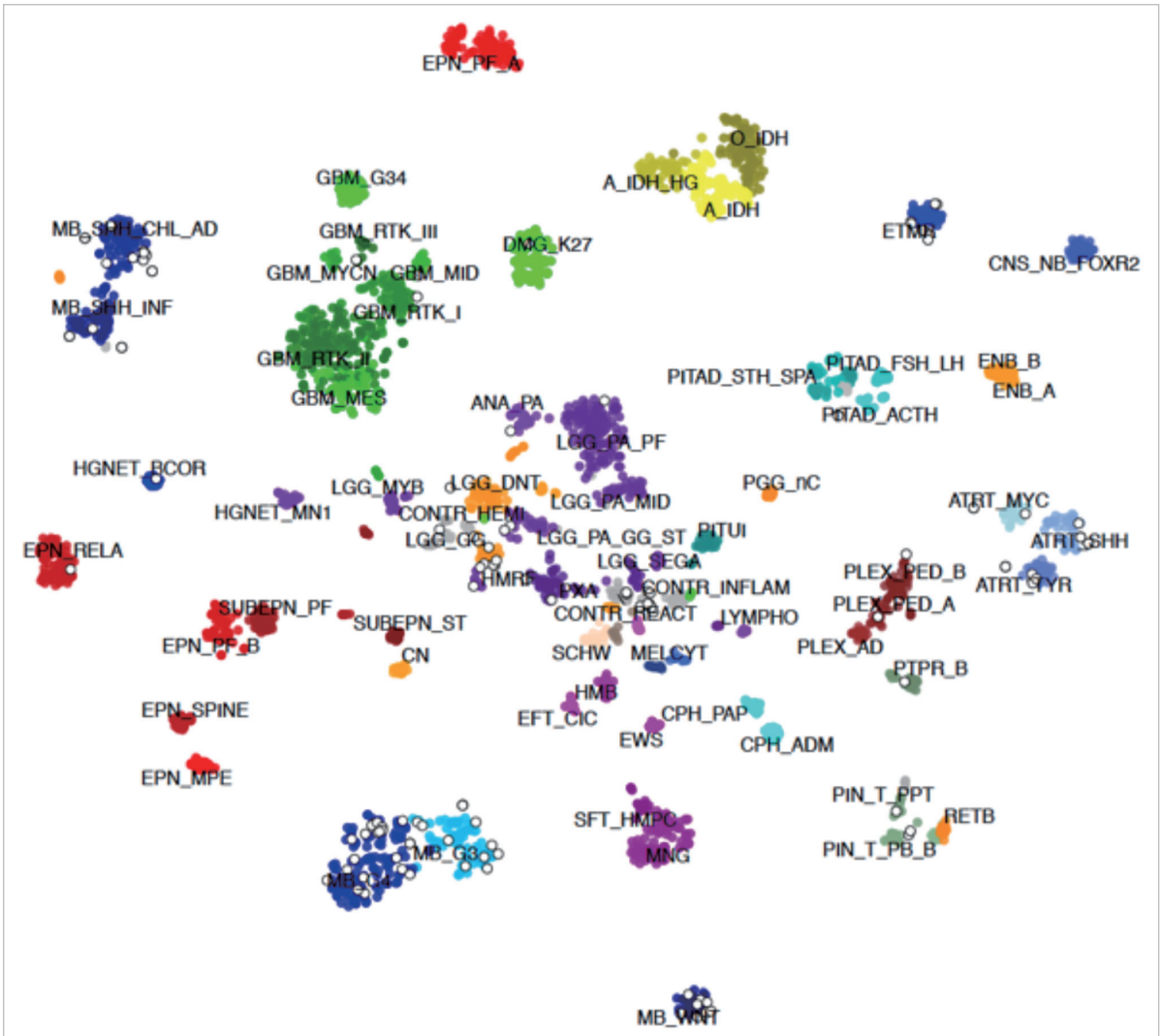

FIG 2. t-SNE analysis comparing the methylation profiles of our cohort (n=97, open white circles) and a publicly available central nervous system (CNS) tumour reference cohort (n=2801, coloured circles), indicating associations between samples and known molecular subclasses of CNS tumours with infrequent outliers

involving a defective array chip. We focused on the main cohort of CNS embryonal/high-grade neuroepithelial tumours.

Among the cohort of 97 samples, DNA was extracted from FFPE slides (n=75), scrolls (n=3), or a combination of the two (n=19). Seven samples required macrodissection to enrich tumour material because of low tumour content. The median quantity of total DNA extracted was 490 (range, 12.5-7290) ng. Up to 500 ng of DNA from each sample were submitted for methylation array analysis.

The cohort samples were from 59 male patients and 38 female patients. The median age at diagnosis was 5.7 (range, 0.6-22.2) years, and the median duration of follow-up was 4.6 (range, 0-20.6) years. Primary tumour locations were the cerebellar/posterior fossa (n=71), cerebral cortex (n=15), pineal gland (n=7), sellar/parasellar regions (n=2), ventricles (n=1), and spine (n=1). Metastasis was documented in 15% of the patients. Among patients with outcomes available (n=85), events occurred in 49; 47 events were tumour related.

The original clinicopathologic diagnoses included medulloblastoma (n=65), ATRT (n=9), pineal parenchymal tumour (n=8), ETMR (n=6), HGNET (n=4), CNS-PNET (n=4), and choroid plexus tumour (n=1). Random forest classifier assessment revealed calibrated scores of >0.9 (confident assignment) in 64 (65%) samples and >0.6 (confident and potentially relevant assignment) in 73 (75%) samples. Unsupervised t-SNE analysis based on a CNS tumour reference cohort (n=2801)[3] indicated that 85 (88%) samples had informative methylation profiles (Fig 2). The methylation-based

TABLE. Methylation-based assignment of central nervous system (CNS) embryonal tumours

Molecular entity	No. of samples (n=97)
Medulloblastoma	52
WNT-activated	8
SHH-activated (infant)	3
SHH-activated (children/adult)	10
Group 3	10
Group 4	21
Atypical teratoid/rhabdoid tumour	9
TYR	5
SHH	3
MYC	1
Pineal parenchymal tumour	6
Pineoblastoma	3
Pineal parenchymal tumour of intermediate differentiation	2
Papillary tumour of the pineal region	1
Embryonal tumour with multi-layered rosettes	7
Pituitary blastoma	2
High-grade neuroepithelial tumour, BCOR-altered	1
High-grade glioma	4
Others	4
Control/no match	12

assignments of samples are summarised in the Table.

Epigenomic profiling allowed molecular subgrouping and confirmation of diagnosis in 65 (67%) samples, confirmation of diagnosis in eight (8%) samples, and suggested alternative diagnosis in 12 (12%) samples. Among the remaining samples (n=12, 12%), four were molecularly similar to reference controls, suggesting non-neoplastic cell contamination, and eight did not cluster with any known references in the classifier or t-SNE analyses. Novel clinicopathologic-molecular associations were established, including an expanded clinical-molecular profile for the rare entity of pituitary blastoma.

Patient outcomes significantly differed according to molecular diagnoses. Patients with better prognosis included individuals with medulloblastoma in the WNT-activated, SHH-activated (children/adult subtype), and group 4 subgroups, which represented 'good-risk' entities. Patients with suboptimal outcomes included patients with medulloblastoma in the SHH-activated (infant subtype) and group 3 subgroups, ETMR, and high-grade glioma.

Discussion

Embryonal tumours, the most common CNS tumours in young children, constitute aggressive WHO Grade IV tumours with a tendency to metastasise. Recent epigenomic studies have revealed that various subtypes of CNS embryonal tumours (ie, medulloblastoma, CNS-PNET, pineoblastoma, and ATRT) are biologically distinct, with intertumoural heterogeneity within subtypes. The present study provides relevant data to support the use of methylation profiling for clinical management of children with CNS neoplasms in Hong Kong.

Molecular assays are often hindered by the difficulty of obtaining good-quality data based on FFPE-derived tumour DNA.[4] Our experience indicated that even when the quantity of DNA is suboptimal (<500 ng), there is value in proceeding with quantitative polymerase chain reaction–based quality control and downstream workflows. In our cohort, 88% of the samples were clustered with established tumour entities. Suboptimal classification is likely related to the predefined structure of current tumour classifiers, suggesting that success rates in methylation studies will continue to improve.

Paediatric patients with cancer in Hong Kong receive uniform treatment. Thus, the correlation between tumour classification and treatment outcomes allowed assessment of prognostic value in each molecular group. Medulloblastoma can be molecularly classified into WNT-activated, SHH-activated, group 3, and group 4 diseases.[5] The superior outcomes among patients with WNT-activated tumours and the aggressiveness of group 3 disease support treatment de-escalation and intensification, respectively. Among our cohort, 12% of samples were re-assigned to an alternative diagnosis. This percentage is similar to that in German and Dutch cohorts. Patients with tumours re-classified as high-grade gliomas had poor survival. Identification of novel entities/associations highlights the challenges in CNS tumour diagnostics based on existing pipelines.

Methylation arrays in tumour diagnostics are dependent on the quality, size, and complexity of the reference cohort with which study samples are compared. For example, CNS germ cell tumours are underrepresented in existing reference sets because of their low incidence in Western populations. To further enhance this epigenetics-based algorithm, multi-national collaborations and evaluations by expert neuropathologists should include integrated interpretation of clinical information, histomorphology, immunohistochemical profiles, and other targeted molecular studies.

Conclusion

DNA methylation profiling is useful in the diagnosis

of paediatric CNS embryonal tumours. Our cohort, one of the largest in Asia, provides a foundation for regional and international collaborations in paediatric neuro-oncology research.

Funding

This study was supported by the Health and Medical Research Fund, Health Bureau, Hong Kong SAR Government (#06171666). The full report is available from the Health and Medical Research Fund website (https://rfs2.healthbureau.gov.hk).

Disclosure

The results of this research have been previously published in:

1. Tam OCH, Ho RSL, Chan S, et al. Genome-wide DNA methylation profiling as frontline diagnostics for central nervous system embryonal tumors in Hong Kong. Cancers (Basel) 2023;15:4880.
2. Liu AP, Li KK, Chow C, et al. Expanding the clinical and molecular spectrum of pituitary blastoma. Acta Neuropathol 2022;143:415-7.
3. Liu AP, Zhen Z, Yang Q, et al. Treatment barriers and clinical outcome of children with medulloblastoma in China: a report from the Chinese Children's Cancer Group (CCCG). Neurooncol Adv 2021;3:vdab134.
4. Yang RR, Li KK, Liu APY, et al. Low-grade BRAF V600E mutant oligodendroglioma-like tumors of children may show EGFR and MET amplification. Brain Pathol 2021;31:211-4.

Acknowledgements

We thank Dr Ronnie SL Ho from Department of Pathology, Queen Mary Hospital and other contributing pathologists, as well as research team members Mr Otto Tam, Dr Shing Chan, and Miss Jasmine Lee for their input. We acknowledge the expert multidisciplinary clinical management provided for patients in the study.

References

1. Ostrom QT, Cioffi G, Gittleman H, et al. CBTRUS statistical report: primary brain and other central nervous system tumors diagnosed in the United States in 2012-2016. Neuro Oncol 2019;21(Suppl 5):v1-v100.
2. Kumar R, Liu APY, Orr BA, Northcott PA, Robinson GW. Advances in the classification of pediatric brain tumors through DNA methylation profiling: from research tool to frontline diagnostic. Cancer 2018;124:4168-80.
3. Capper D, Jones DT, Sill M, et al. DNA methylation-based classification of central nervous system tumours. Nature 2018;555:469-74.
4. Hovestadt V, Remke M, Kool M, et al. Robust molecular subgrouping and copy-number profiling of medulloblastoma from small amounts of archival tumour material using high-density DNA methylation arrays. Acta Neuropathol 2013;125:913-6.
5. Northcott PA, Buchhalter I, Morrissy AS, et al. The whole-genome landscape of medulloblastoma subtypes. Nature 2017;547:311-7.

Faecal microbiota transplantation for patients with irritable bowel syndrome: abridged secondary publication

YK Yau, Q Su, Z Xu, W Tang, JYL Ching, CP Cheung, M Fung, M Ip, PKS Chan, FKL Chan, SC Ng *

KEY MESSAGES

1. Faecal microbiota transplantation, delivered twice at an interval of 4 weeks, was not associated with overall improvement in irritable bowel syndrome symptoms.
2. Faecal microbiota transplantation relieved the most annoying symptom—abdominal bloating—likely by reducing hydrogen sulphide–producing bacteria in the gut.
3. Additional studies are needed to determine the optimal regimen.

Hong Kong Med J 2024;30(Suppl 1):S34-8
HMRF project number: 06170576

[1,2,3] YK Yau, [1,2,3] Q Su, [1,2,3] Z Xu, [1,2,3] W Tang, [1,2] JYL Ching, [1,2,3] CP Cheung, [1,2,3] M Fung, [4] M Ip, [4] PKS Chan, [1,2,3] FKL Chan, [1,2,3] SC Ng

[1] *Department of Medicine and Therapeutics, The Chinese University of Hong Kong, Hong Kong SAR, China*
[2] *Microbiota I-Center (MagIC), Hong Kong SAR, China*
[3] *Li Ka Shing Institute of Health Sciences, State Key Laboratory of Digestive Disease, Institute of Digestive Disease, The Chinese University of Hong Kong, Hong Kong SAR, China*
[4] *Department of Microbiology, The Chinese University of Hong Kong, Hong Kong SAR, China*

YK Yau and Q Su contributed equally
* Principal applicant and corresponding author: siewchienng@cuhk.edu.hk

Introduction

Irritable bowel syndrome (IBS) is a common gastrointestinal disorder worldwide. Observational studies have shown that faecal microbiota transplantation (FMT) delivered via the upper or lower gastrointestinal tract improves IBS symptoms, but randomised trials have yielded conflicting results.[1] An observational study revealed that seven of 10 patients with IBS achieved significant clinical improvement after a second dose of FMT,[2] suggesting that a second dose of FMT can enhance the therapeutic response.

The composition of faecal microbes in patients with IBS may affect the therapeutic efficacy of FMT. Some studies have identified certain bacteria and their metabolites, such as *Bacteroides* and butyric acid, as key determinants of the treatment response after FMT.[3] However, most published microbiota profiles have been based on the 16S RNA sequencing. The mechanism by which FMT relieves specific symptoms of IBS is unknown.

We hypothesised that FMT could relieve specific IBS symptoms by modulating the gut microbiota. We assessed the efficacy of FMT, delivered twice at an interval of 4 weeks, in relieving symptoms of IBS. We also explored associations between changes in gut microbiota signatures and clinical symptoms.

Methods

In this randomised, double-blind, placebo-controlled study, patients with IBS meeting the Rome III criteria were randomly assigned (in a 1:1 ratio) to receive frozen FMT from healthy donors or placebo via the duodenal route at baseline and week 4. Patients were assessed at baseline, week 4, week 8, and week 12 using a questionnaire. The primary outcome was clinical response, defined as a decrease of ≥75 points in the IBS severity scoring system (IBS-SSS). Secondary outcomes were improvement in general symptoms and improvement in bloating at week 12. After the trial, open-label FMT was provided for patients who had received placebo.

Stool samples were collected at baseline, week 4, week 8, and week 12 for DNA extraction. Extracted DNA was used to construct DNA libraries. Raw sequence data were quality-filtered to remove adaptors, low-quality sequences (quality score <20), and reads shorter than 50 base pairs. Contaminating reads were filtered with default parameters. Microbiota profiles were inferred from quality-filtered forward reads; species with average abundance <0.15% and prevalence <5% were filtered out. Microbiota functional annotation was then profiled.

Continuous data were compared using the Mann-Whitney *U* test, and categorical variables were compared using the Chi-squared test or Fisher's exact test (expected count <5). Within-group differences in IBS-SSS score over time were compared using repeated measures analysis of variance. Associations of specific microbial species with clinical parameters were identified using the multivariable analysis by linear models.

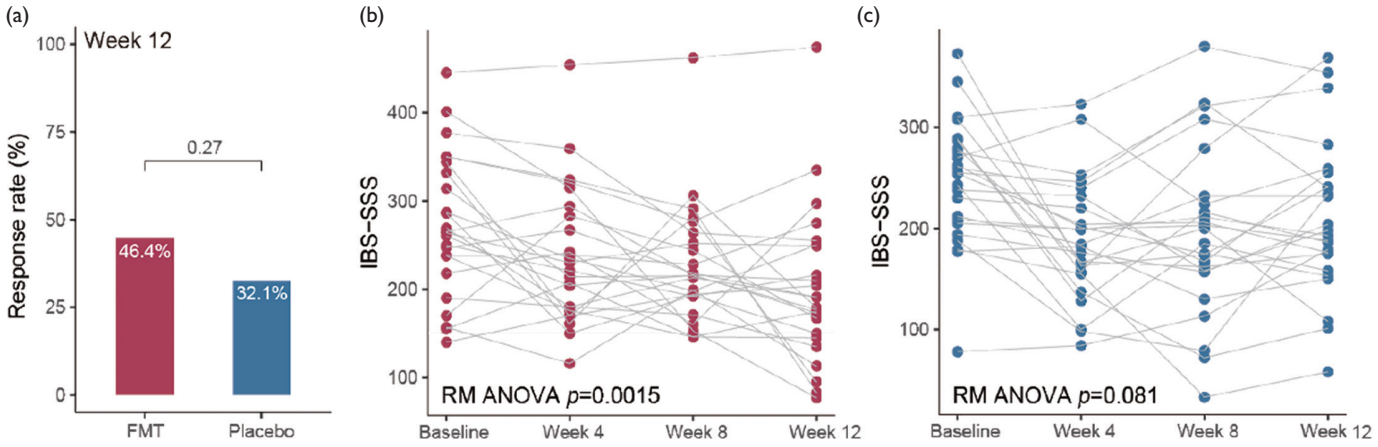

FIG 1. (a) Clinical response at week 12 and irritable bowel syndrome severity scoring system (IBS-SSS) scores over 12 weeks in (b) faecal microbiota transplantation (FMT) and (c) placebo arms

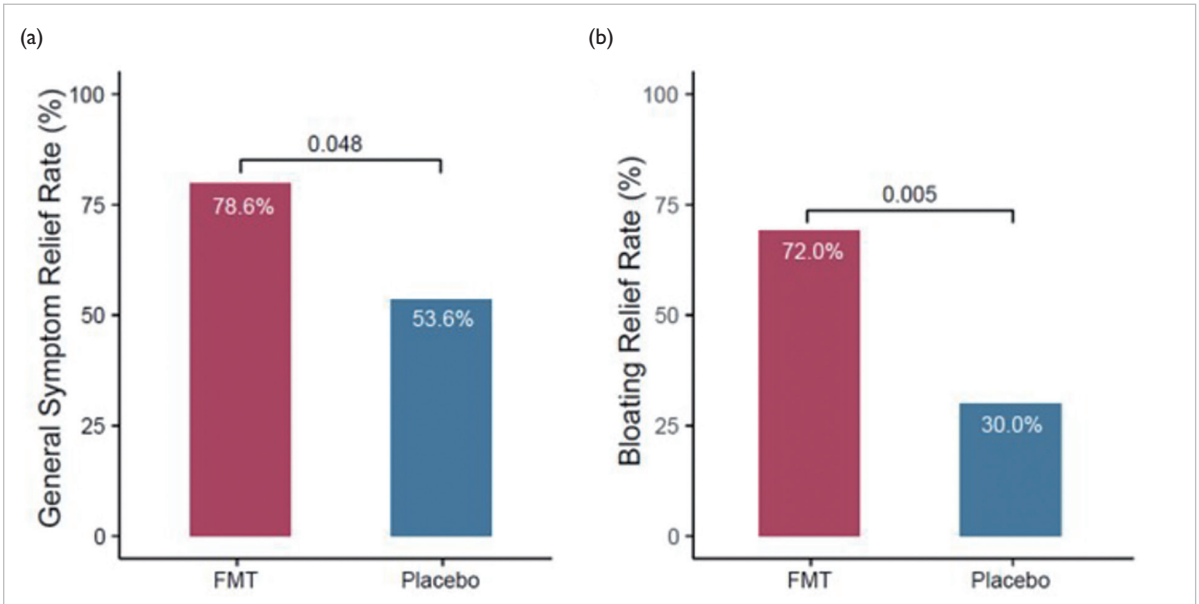

FIG 2. Self-reported (a) general symptom and (b) bloating relief rates at week 12 in faecal microbiota transplantation (FMT) and placebo arms

Results

Between April 2017 and September 2021, 56 patients with diarrhoea-dominant IBS were randomly assigned to receive FMT (n=28) or placebo (n=28). At week 12, 13 (46.4%) patients in the FMT arm and nine (32.1%) patients in the placebo arm had clinical response (P=0.27, Fig 1). Patients in the FMT arm showed a significant reduction in IBS-SSS score (P=0.0015), whereas no significant change was observed in the placebo arm (P=0.081). Higher proportion of patients in the FMT arm had improvements in self-reported general symptoms of IBS (78.6% vs 53.6%, P=0.048) and abdominal bloating (72% vs 30%, P=0.005) [Fig 2]. The two arms were comparable in terms of stool consistency, abdominal pain, IBS-quality of life score, or Generalised Anxiety Disorder-7 score. Clinical response was achieved in seven (30.4%) of 23 patients in the FMT arm, with improvements in IBS-SSS score (P=0.00067), IBS-quality of life score

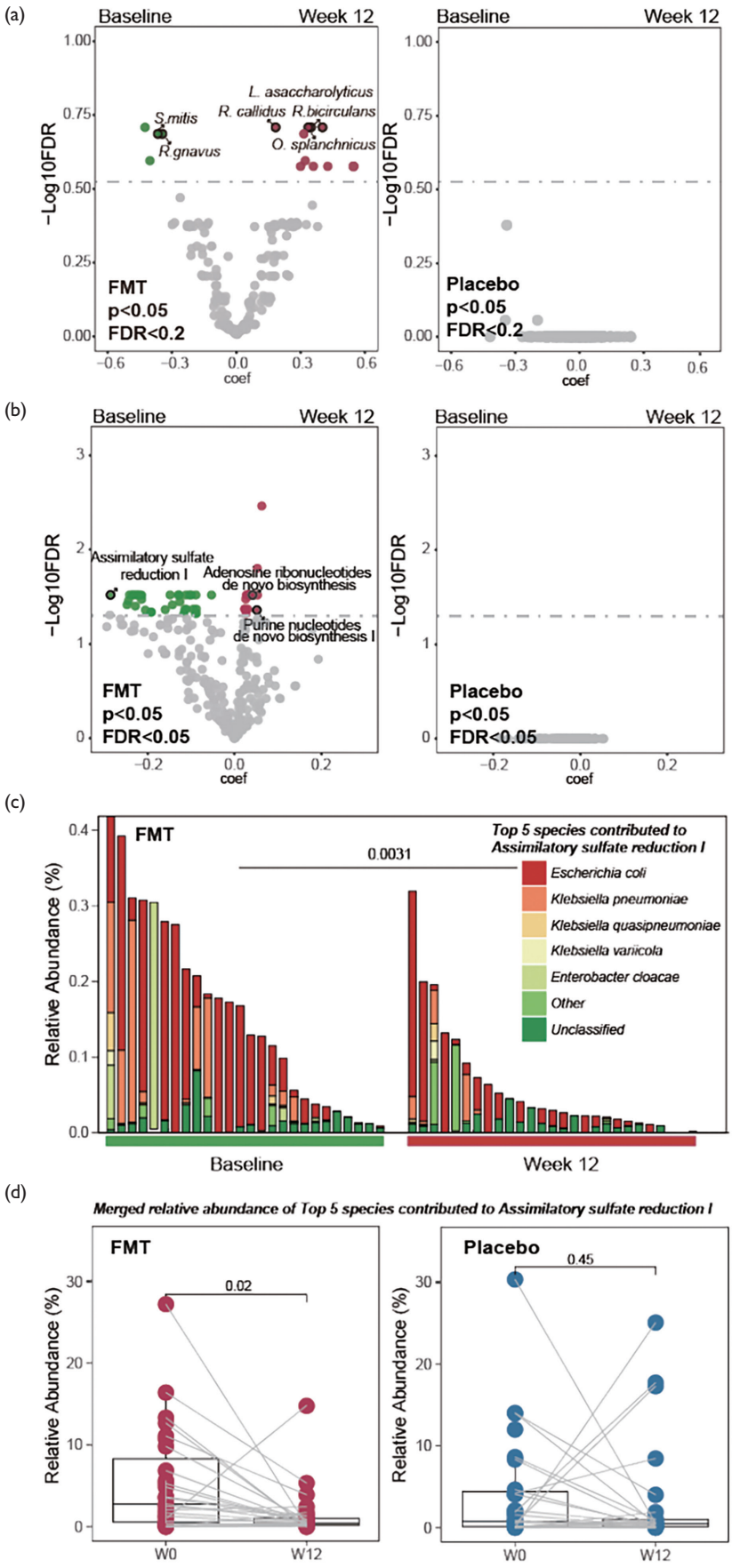

FIG 3. Faecal microbiota (a) composition at species level and (b) functional dynamics from baseline to week 12 in faecal microbiota transplantation (FMT) and placebo arms. False discovery rate (FDR) of <0.2 was considered statistically significant. (c) Contributions and (d) merged relative abundance of top five bacterial species to the assimilatory sulphate reduction I pathway.

(P=0.03), Generalised Anxiety Disorder-7 score (P=0.011), and abdominal pain (P=0.026), compared with baseline. Additionally, general symptom relief and bloating relief were achieved by 73.9% and 82.4%, respectively, of patients receiving open-label FMT at week 12.

Faecal microbial diversity (Shannon) and richness (observed number of species) did not significantly change from baseline to week 12 in the FMT or placebo arm (P>0.05). At week 12, the gut microbiota profile among patients in the FMT arm did not significantly shift toward the profile of the donors (P>0.05) but showed a significantly greater dissimilarity relative to baseline, compared with patients in the placebo arm (assessed by Bray-Curtis dissimilarity, P=0.03). Importantly, among patients who received FMT, the abundances of several potential beneficial bacteria (eg, *Lawsonibacter asaccharolyticus*, *Ruminococcus bicirculans*, *Odoribacter splanchnicus*, and *Ruminococcus callidus*) were significantly increased, whereas the abundances of several pro-inflammatory bacteria (eg, *Ruminococcus gnavus* and *Streptococcus mitis*) were significantly decreased (P<0.05, false discovery rate <0.2, Fig 3). However, no significant change at the species level was observed in the placebo arm at week 12, compared with baseline. In the FMT arm, the relative abundances of 22 metabolic pathways were significantly increased and those of 34 pathways were significantly decreased at week 12, compared with baseline (false discovery rate <0.05). The metabolic pathway with the greatest reduction in patients who received FMT was assimilatory sulphate reduction I, which produces hydrogen sulphide and may contribute to bloating. The top bacterial species that contribute to the assimilatory sulphate reduction I pathway were identified as *Escherichia coli* and several *Klebsiella* spp (Fig 3). There was a significant decrease in the total relative abundance of these bacteria in the FMT arm (P=0.02), but no significant change was evident in the placebo arm.

Discussion

Although FMT received twice at an interval of 4 weeks did not result in significant improvement in global IBS symptoms as measured by the IBS-SSS score, it improved abdominal bloating by >2-fold and self-reported general symptoms by 1.5-fold at week 12. This sustained improvement could be explained by the changes in the gut microbiota; FMT led to inhibition of gas-producing bacterial pathways and reduced abundances of hydrogen sulphide–producing bacteria in the gut. Our metagenomic analysis of bacterial functional pathways may provide a plausible biological explanation for this. Patients with IBS have higher faecal abundances of *E coli* and several *Klebsiella* spp, compared with non-IBS controls.[4] These putative pathogens may contribute to intestinal production of hydrogen sulphide, which can cause diarrhoea and bloating. Hydrogen sulphide is also a potential biomarker for small intestinal bacterial overgrowth in diarrhoea-predominant IBS.[5] Our results showed that FMT significantly decreased hydrogen sulphide production by reducing the abundances of *E coli* and several *Klebsiella* spp, which may partly explain significant relief from abdominal bloating. We speculate that FMT can be beneficial for a specific subgroup of patients with IBS whose predominant symptom is abdominal bloating.

This study had some limitations. First, it was not designed to target patients with IBS who report bloating. A larger sample size involving more homogenous patients with IBS who report bloating is needed to confirm our findings. Second, we speculate that the bloating improvement was related to the reduced abundances of hydrogen sulphide–producing bacteria. Animal experiments are required to confirm this mechanism. Third, analyses according to IBS subtype were not performed because of the limited sample size. Fourth, the sample size and number of donors were not sufficient to assess the donor effect on the efficacy of FMT for treating IBS. Optimisation of donor-recipient pairing may further improve the clinical response rate. Further research is needed to determine the optimal selection criteria for FMT candidates and optimal microbiota profiles of donors. Fifth, symptoms of abdominal distension or bloating were self-reported by patients; objective assessments, such as breath tests, would provide more insights. Sixth, we did not compare FMT with other treatment options (eg, training in abdominal relaxation techniques). Further research involving additional objective assessments and comparisons with other treatment options is needed to guide clinical applications of FMT in IBS treatment.

Conclusions

In patients with IBS whose predominant symptom is abdominal bloating, FMT is a safe, feasible, and effective treatment, probably owing to reduced abundances of hydrogen sulphide–producing bacteria in the gut. Our findings may help policymakers, health service managers, and service providers develop guidelines and implement FMT services in hospitals. Future studies should focus on patient selection, dosing regimens, and cost-effectiveness.

Funding

This study was supported by the Health and Medical Research Fund, Health Bureau, Hong Kong SAR Government (#06170576). The full report is available from the Health and Medical Research Fund website (https://rfs2.healthbureau.gov.hk).

Disclosure

The results of this research have been previously published in:

1. Yau YK, Su Q, Xu Z, et al. Randomised clinical trial: faecal microbiota transplantation for irritable bowel syndrome with diarrhoea. Aliment Pharmacol Ther 2023;58:795-804.
2. Su Q, Yau YK, Ng SC. Editorial: Faecal microbiota transplantation in IBS-Moving closer or away from success? Authors' reply. Aliment Pharmacol Ther 2023;58:952-3.

References

1. Elhusein AM, Fadlalmola HA. Efficacy of fecal microbiota transplantation in irritable bowel syndrome patients: an updated systematic review and meta-analysis. Gastroenterology Nursing 2022;45:11-20.
2. El-Salhy M, Hausken T, Hatlebakk JG. Increasing the dose and/or repeating faecal microbiota transplantation (FMT) increases the response in patients with irritable bowel syndrome (IBS). Nutrients 2019;11:1415.
3. El-Salhy M, Kristoffersen AB, Valeur J, et al. Long-term effects of fecal microbiota transplantation (FMT) in patients with irritable bowel syndrome. Neurogastroenterol Motil 2022;34:e14200.
4. Ganji L, Alebouyeh M, Shirazi MH, et al. Dysbiosis of fecal microbiota and high frequency of Citrobacter, Klebsiella spp., and Actinomycetes in patients with irritable bowel syndrome and gastroenteritis. Gastroenterol Hepatol Bed Bench 2016;9:325-330.
5. Banik GD, De A, Som S, et al. Hydrogen sulphide in exhaled breath: a potential biomarker for small intestinal bacterial overgrowth in IBS. J Breath Res 2016;10:026010.

Perceptual learning for adults with astigmatism-related amblyopia: abridged secondary publication

TW Leung *, CS Kee, RWH Li

KEY MESSAGES

1. Perceptual learning to detect gratings at near cut-off spatial frequencies can improve grating acuity, visual acuity, and stereoacuity while alleviating meridional visual deficits in adults with amblyopia.
2. Occlusion therapy provided minimal visual benefits for adults with amblyopia.
3. Perceptual learning did not improve visual function in normally sighted adults.

Hong Kong Med J 2024;30(Suppl 1):S39
HMRF project number: 02160117

[1] **TW Leung,** [1] **CS Kee,** [2] **RWH Li**

[1] *School of Optometry, The Hong Kong Polytechnic University, Hong Kong SAR, China*
[2] *School of Optometry, University of California Berkeley, United States*

* Principal applicant and corresponding author: jeffrey.tw.leung@polyu.edu.hk

Introduction

Uncorrected astigmatism during critical periods in children can disrupt normal visual development, potentially leading to persistent visual impairment known as meridional amblyopia or astigmatism-related amblyopia. The traditional first-line intervention for this condition involves the prescription of corrective spectacles. However, optical correction alone or in combination with occlusion therapy is not always sufficient to fully restore vision,[1] particularly in young children of kindergarten age. Consequently, there is a pressing need for more effective treatment modalities.

Traditional approaches to amblyopia treatment typically target individuals before the age of 8 years, which is considered the critical period for visual development. Nevertheless, recent research indicates that intensive vision therapy can induce neural plasticity in adults with strabismic and anisometropic amblyopia.[2-4] In light of these findings, we propose a treatment strategy for the specific visual deficits associated with astigmatism to correct this type of brain-related visual disorder. Our study aims to establish a training regimen to enhance grating acuity along the most impaired meridian in individuals with astigmatism-related amblyopia.

Methods

A cohort of 35 patients diagnosed with amblyopia was randomly allocated to receive either perceptual learning therapy (n=19) or occlusion therapy (n=16). Perceptual learning to detect gratings at near cut-off spatial frequencies was used to treat adults with astigmatism-related amblyopia.

Results

After 20 hours of training over 4 weeks, participants showed 24% improvement in grating acuity, 65% improvement in meridional anisotropy, 38% improvement in visual acuity, and 16% improvement in stereoacuity. In contrast, patients receiving occlusion therapy did not exhibit significant improvement in any of these visual functions. Perceptual learning did not improve visual function in normally sighted adults.

Discussion

These findings highlight the potential for perceptual learning to activate neural plasticity and ameliorate visual deficits in adults with amblyopia who have exceeded the age window corresponding to the critical period of visual development. The ability of targeted learning therapy (rather than optical correction of refractive errors) to treat the underlying astigmatism-related functional impairment represents a promising direction for amblyopia care.

Funding

This study was supported by the Health and Medical Research Fund, Health Bureau, Hong Kong SAR Government (#02160117). The full report is available from the Health and Medical Research Fund website (https://rfs2.healthbureau.gov.hk).

References

1. Harvey EM. Development and treatment of astigmatism-related amblyopia. Optom Vis Sci 2009;86:634-9.
2. Li RW, Levi DM. Characterizing the mechanisms of improvement for position discrimination in adult amblyopia. J Vis 2004;4:476-87.
3. Li RW, Klein SA, Levi DM. Prolonged perceptual learning of positional acuity in adult amblyopia: perceptual template retuning dynamics. J Neurosci 2008;28:14223-9.
4. Li RW, Ngo C, Nguyen J, Levi DM. Video-game play induces plasticity in the visual system of adults with amblyopia. PLoS Biol 2011;9:e1001135.

Glaucoma secondary to vascular changes in optic nerve head, retina, and choroid: abridged secondary publication

CCY Tham *, PPM Chan, CYL Cheung, DYL Leung, NCY Chan, CWY Chow

KEY MESSAGES

1. Decreased vessel density is associated with impaired visual sensitivity in the early stage of normal-tension glaucoma.
2. Patterns of retinal vasculature changes differ between normal-tension glaucoma and primary angle-closure glaucoma.
3. Lower retinal vasculature density at baseline is associated with faster progression of normal-tension glaucoma.
4. Vascular changes develop prior to retinal nerve fibre layer (RNFL) thinning in normal-tension glaucoma, whereas RNFL thinning develops prior to vascular changes in primary angle-closure glaucoma.

Hong Kong Med J 2024;30(Suppl 1):S40-44
HMRF project number: 05162836

CCY Tham, PPM Chan, CYL Cheung, DYL Leung, NCY Chan, CWY Chow

Department of Ophthalmology and Visual Sciences, The Chinese University of Hong Kong, Hong Kong SAR, China

* Principal applicant and corresponding author: clemtham@cuhk.edu.hk

Introduction

Glaucoma is a major cause of irreversible blindness worldwide.[1] It is characterised by retinal ganglion cell (RGC) degeneration, which results in thinning of the optic disc and retinal nerve fibre layer (RNFL) as well as visual field loss. The pathogenesis of glaucoma remains unknown. Intraocular pressure (IOP) reduction is the only effective therapeutic strategy to slow glaucoma progression, but some patients experience continued progression despite clinically significant IOP reduction.

Various vascular mechanisms such as decreased perfusion pressure, vascular dysregulation, and vasospasm may involve in the pathogenesis and progression of glaucoma.[2,3] Both IOP and vascular factors are likely to cause high-tension glaucoma (primary open-angle glaucoma and primary angle-closure glaucoma [PACG]) and normal-tension glaucoma (NTG). Retinal arteriolar narrowing is associated with the 10-year incidence of glaucoma, independent of IOP and ocular perfusion pressure.[4]

Optical coherence tomography angiography (OCT-A) enables quantitative evaluation of retinal and choroidal microvasculature. Microvascular reduction is associated with visual field defects and RGC loss in glaucoma. We used OCT-A to quantify capillary networks and evaluate the causal relationship between retinal vascular changes and RGC loss in glaucoma.

Methods

This study was conducted from 1 April 2018 to 31 July 2022. Patients with glaucoma and healthy controls were consecutively recruited for ophthalmic examinations of visual acuity, IOP, refraction, axial length, and visual field, using dark-room gonioscopy, OCT, and OCT-A imaging. All patients with glaucoma were followed up every 6 months.

OCT-A imaging was performed using a volume scan over a 3×3-mm macular region centred on the optic nerve head and the fovea. In the macular region, only the superficial capillary plexus was analysed because the deep capillary plexus can be affected by shadow graphical projection artefacts from the superficial capillary plexus. In the optic disc region, only the radial peripapillary capillary layer was analysed because this layer contains the blood supply for the RNFL layer. A customised MATLAB programme was used to process OCT-A images and generate a series of quantitative OCT-A metrics. Multiple quantitative vascular parameters were generated, including vessel density (VD), fractal dimension, and vessel diameter index.

For cross-sectional analyses, generalised estimating equations were used to correct for inter-eye correlations. Linear regression was performed to examine associations between OCT-A metrics and glaucoma parameters. For longitudinal analysis, the rates of change in VD and RNFL thickness were

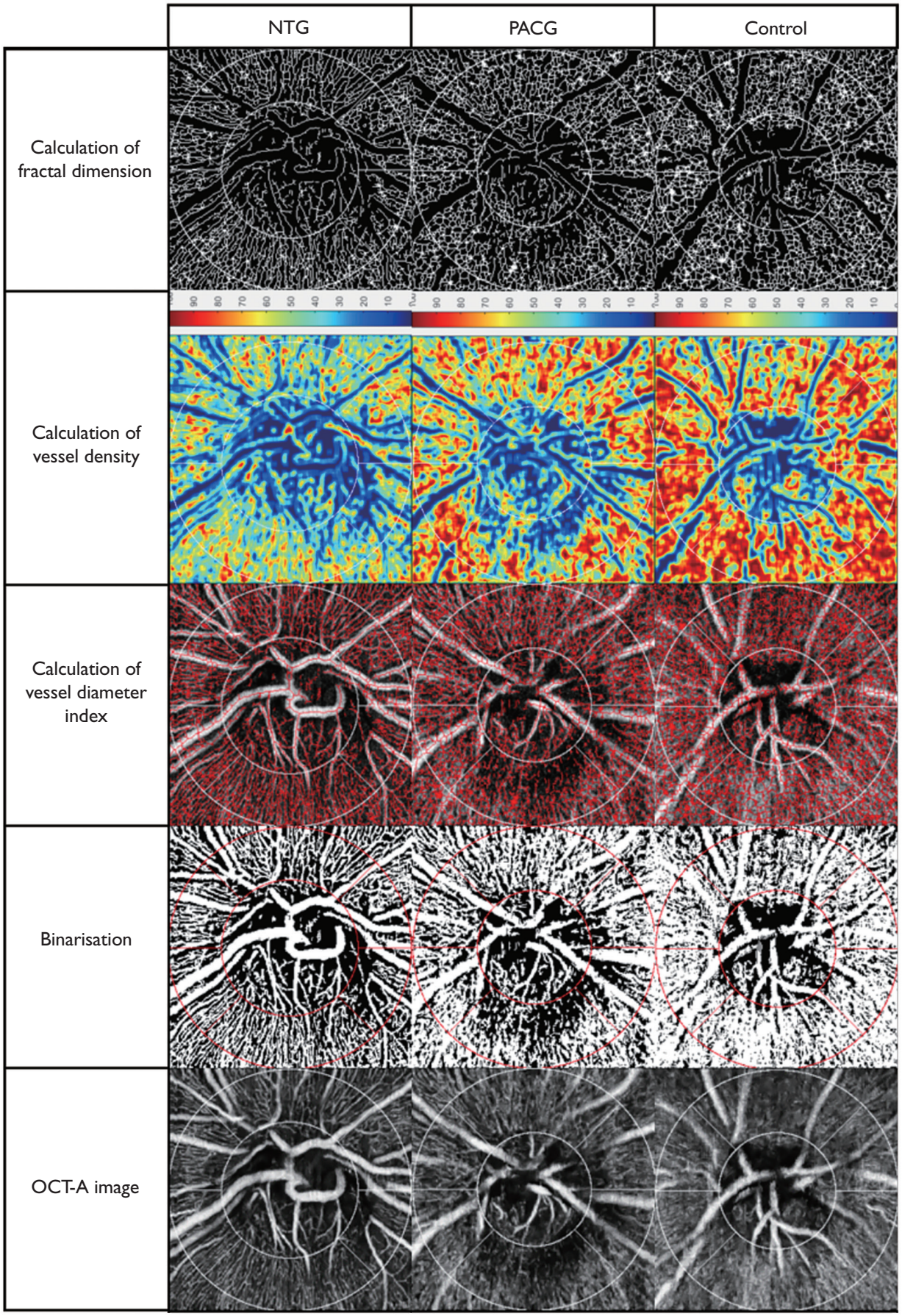

FIG. Quantitative peripapillary microvasculature metrics in optical coherence tomography angiography (OCT-A) images of patients with normal-tension glaucoma (NTG), patients with primary angle-closure glaucoma (PACG), and healthy controls.

TABLE 1. Associations of circumpapillary vessel density (VD) and circumpapillary fractal dimension (FD) with mean retinal nerve fibre layer (RNFL) thickness

Metric	Univariable model*		Multivariable model*	
	RNFL thickness, μm	P value	RNFL thickness, μm	P value
Patients with primary angle-closure glaucoma				
Circumpapillary VD, %	-5.855 (-9.567 to -2.143)	0.002	-4.242 (-8.120 to -0.363)	0.032
Circumpapillary FD	-9.297 (-11.682 to -6.913)	<0.001	-8.894 (-11.925 to -5.864)	<0.001
Patients with normal-tension glaucoma				
Circumpapillary VD, %	-4.998 (-7.674 to -2.322)	<0.001	-5.531 (-9.472 to -1.590)	0.006
Circumpapillary FD	-9.831 (-15.901 to -3.761)	0.002	-12.064 (-17.195 to -6.932)	<0.001
Controls				
Circumpapillary VD, %	1.918 (-0.684 to 4.520)	0.148	2.221 (-0.197 to 4.638)	0.072
Circumpapillary FD	-0.646 (-3.284 to 1.992)	0.631	-1.325 (-3.891 to 1.241)	0.312

* Data are presented as mean (95% confidence interval) per standard-deviation decrease

TABLE 2. Age- and baseline measurement-adjusted rates of change in vessel density and retinal nerve fibre layer thickness

Variables	Patients with normal-tension glaucoma*	P value	Patients with primary angle-closure glaucoma*	P value	Difference*	P value
Vessel density, %/y						
Global	-1.65 (-2.40 to -0.89)	<0.001	-0.66 (-1.32 to -0.01)	0.047	-1.08 (-1.90 to -0.27)	0.009
Temporal	-2.06 (-3.08 to -1.05)	<0.001	-0.49 (-1.36 to 0.38)	0.262	-1.57 (-2.91 to -0.23)	0.022
Superotemporal	-2.23 (-3.39 to -1.08)	<0.001	-0.75 (-1.76 to 0.26)	0.140	-1.46 (-2.65 to -0.26)	0.017
Inferotemporal	-1.63 (-2.77 to -0.49)	0.006	-0.73 (-1.73 to 0.26)	0.143	-0.99 (-2.23 to 0.25)	0.117
Superonasal	-1.09 (-2.19 to 0.00)	0.050	-0.46 (-1.54 to 0.61)	0.394	-0.86 (-2.09 to 0.38)	0.172
Inferonasal	-1.61 (-2.80 to -0.41)	0.009	-1.25 (-2.58 to 0.09)	0.067	-0.67 (-2.03 to 0.69)	0.334
Nasal	-1.39 (-2.37 to -0.42)	0.006	-0.67 (-1.57 to 0.23)	0.138	-0.74 (-1.81 to 0.34)	0.178
Retinal nerve fibre layer thickness, μm/y						
Global	-0.25 (-0.92 to 0.43)	0.467	-0.62 (-1.14 to -0.10)	0.020	0.41 (-0.48 to 1.30)	0.360
Temporal	-0.33 (-1.10 to 0.44)	0.399	-0.45 (-1.03 to 0.13)	0.127	0.12 (-0.85 to 1.09)	0.801
Superotemporal	-1.11 (-2.06 to -0.17)	0.022	-0.43 (-1.34 to 0.48)	0.354	-0.72 (-2.03 to 0.58)	0.276
Inferotemporal	-1.76 (-2.79 to -0.73)	0.001	-0.97 (-1.79 to -0.16)	0.019	-0.63 (-1.95 to 0.68)	0.342
Superonasal	-0.89 (-1.59 to -0.18)	0.013	-0.96 (-1.82 to -0.11)	0.028	0.07 (-0.95 to 1.10)	0.889
Inferonasal	-0.75 (-1.75 to 0.25)	0.138	-0.84 (-1.70 to 0.01)	0.053	0.03 (-1.28 to 1.34)	0.969
Nasal	-0.30 (-1.35 to 0.75)	0.569	-0.37 (-0.95 to 0.20)	0.197	0.05 (-1.13 to 1.23)	0.933

* Data are presented as coefficient (95% confidence interval)

estimated by linear mixed-effects modelling. Mean differences in rates of change between diagnostic groups were compared by linear mixed-effects modelling.

Results

In total, 250 patients with NTG, 250 patients with PACG, and 130 healthy controls were recruited. Their quantitative peripapillary microvasculature metrics on OCT-A were compared (Fig). Decreased circumpapillary VD and circumpapillary fractal dimension were associated with decreased RNFL thickness in both NTG and PACG groups (all P≤0.032, Table 1). The associations between OCT-A metrics and RNFL thickness were stronger in the NTG group than in the PACG group.

In the NTG group, the rate of VD loss was significantly different from zero in each sector and global region (all P≤0.05); the rate of RNFL thinning was significantly different from zero in the superotemporal, inferotemporal, and superonasal sectors (P≤0.022) [Table 2]. In the PACG group, the rate of VD loss was significantly different from zero in the global region (P=0.047); the rate of RNFL thinning was significantly different from zero in the inferotemporal and superonasal sectors as well as the global region (all P≤0.028). Compared with the PACG group, the NTG group had more rapid VD loss in the global region (P=0.009), temporal sector (P=0.022), and superotemporal sector (P=0.017).

Discussion

We used OCT-A to compare peripapillary microvasculature between two subtypes of early glaucoma with different pathogeneses: NTG is less IOP-dependent and has a stronger vascular pathogenic component, whereas PACG is more IOP-dependent.[5] Global circumpapillary VD was significantly reduced in NTG eyes, compared with PACG eyes, despite comparable RNFL thickness and disease severity. Furthermore, NTG eyes exhibited significantly lower circumpapillary VDs in the inferotemporal and inferonasal sectors, compared with PACG eyes, despite similar RNFL thicknesses in these sectors. These findings suggest that ocular perfusion change patterns differ between the two glaucoma subtypes.

The rates of RNFL thinning were detectable in the superotemporal, inferotemporal, and superonasal sectors of NTG eyes. Focal RNFL thinning in the superotemporal and inferotemporal sectors corresponds to the initial stages of optic nerve damage in glaucomatous eyes. NTG eyes exhibited substantial VD loss over time in each sector and global region; such loss was more uniform than the observed RNFL thinning. These findings support the hypothesis that glaucomatous RNFL damage is a secondary consequence of insufficient ocular blood supply in NTG. Notably, our results may have been influenced by age-related changes. Based on the relatively short follow-up period, we believe that the rate of change is primarily disease related. Nonetheless, further longitudinal assessment is needed to clarify age-related changes in the VD and RNFL of healthy individuals.

Conclusion

This study provided evidence on the roles of retinal vascular changes in the pathogenesis of different glaucoma subtypes. Further studies are warranted to explore novel interventions based on vascular protection mechanisms.

Funding

This study was supported by the Health and Medical Research Fund, Health Bureau, Hong Kong SAR Government (#05162836). The full report is available from the Health and Medical Research Fund website (https://rfs2.healthbureau.gov.hk).

Disclosure

The results of this research have been previously published in:

1. Lin TPH, Hui HYH, Ling A, et al. Risk of normal tension glaucoma progression from automated baseline retinal-vessel caliber analysis: a prospective cohort study. Am J Ophthalmol 2023;247:111-20.
2. Wang YM, Shen R, Lin TPH, et al. Optical coherence tomography angiography metrics predict normal tension glaucoma progression. Acta Ophthalmol 2022;100:e1455-e1462.
3. Shen R, Wang YM, Cheung CY, et al. Relationship between macular intercapillary area measured by optical coherence tomography angiography and central visual field sensitivity in normal tension glaucoma. Br J Ophthalmol 2023;107:816-22.
4. Shen R, Wang YM, Cheung CY, Chan PP, Tham CC. Comparison of optical coherence tomography angiography metrics in primary angle-closure glaucoma and normal-tension glaucoma. Sci Rep 2021;11:23136.

References

1. Tham YC, Li X, Wong TY, Quigley HA, Aung T, Cheng

CY. Global prevalence of glaucoma and projections of glaucoma burden through 2040: a systematic review and meta-analysis. Ophthalmology 2014;121:2081-90.
2. Leske MC, Wu SY, Hennis A, Honkanen R, Nemesure B; BESs Study Group. Risk factors for incident open-angle glaucoma: the Barbados Eye Studies. Ophthalmology 2008;115:85-93.
3. Armaly MF, Krueger DE, Maunder L, et al. Biostatistical analysis of the collaborative glaucoma study. I. Summary report of the risk factors for glaucomatous visual-field defects. Arch Ophthalmol 1980;98:2163-71.
4. Wu R, Cheung CY, Saw SM, Mitchell P, Aung T, Wong TY. Retinal vascular geometry and glaucoma: the Singapore Malay Eye Study. Ophthalmology 2013;120:77-83.
5. Flammer J, Orgul S, Costa VP, et al. The impact of ocular blood flow in glaucoma. Prog Retin Eye Res 2002;21:359-93.

Aspirin delays the metabolic clock of gestation in women at risk of preeclampsia: abridged secondary publication

CYL Poon *, TY Leung, CC Wang, S Daljit, K Nicolaides, F Scaglia, KYY Cheng, A Milosavljevic

KEY MESSAGES

1. Aspirin significantly delays the metabolic clock according to estimated gestational age.
2. Aspirin treatment partially reverses a wide range of metabolic changes during gestation.
3. These results strongly support the aspirin-related delay hypothesis.

Hong Kong Med J 2024;30(Suppl 1):S45-6
HMRF project number: 06171046

[1] CYL Poon, [1] TY Leung, [1] CC Wang, [1] S Daljit, [2] K Nicolaides, [3] F Scaglia, [1] KYY Cheng, [3] A Milosavljevic

[1] *Department of Obstetrics and Gynaecology, The Chinese University of Hong Kong, Hong Kong SAR, China*
[2] *Fetal Medicine Research Institute, Harris Birthright Centre, King's College London, London, United Kingdom*
[3] *Department of Molecular and Human Genetics, Baylor College of Medicine, Houston, Texas, United States*

* Principal applicant and corresponding author: liona.poon@cuhk.edu.hk

Introduction

Low-dose aspirin treatment can reduce the rate of preterm preeclampsia in high-risk women, but the mechanism underlying the prophylactic response is unknown. Exploratory analyses have suggested that aspirin can delay placental ageing and thus the onset of preeclampsia. We aim to investigate the effects of aspirin on gestational age advancement and the risk of preeclampsia using a molecular estimator specific to high-risk pregnant women.

Methods

This study used plasma samples from the ASPRE trial involving pregnant women at high risk for preterm preeclampsia. Plasma samples were collected at 11 to 13 weeks (before treatment) and at 20 to 23 weeks (after treatment). Untargeted metabolomics profiling was performed on plasma samples from 58 women in the aspirin group and 58 women in the placebo group. Each treatment group contained 30 women who eventually developed preeclampsia and 28 women who did not. Samples from each of the four treatment/outcome combinations were matched approximately 1:1:1:1 according to predicted preeclampsia risk scores.

Results

Metabolic effects of aspirin and metabolic differences were potentially associated with variation in the treatment response. Aspirin treatment resulted in a strong drug-associated metabolomics signature, and the preeclamptic or non-preeclamptic outcome in response to treatment was associated with the level of internal aspirin exposure (P=0.0083). Comparing women with and without preeclampsia after aspirin treatment revealed differences in 73 metabolites, some of which are involved in pathways with regulatory importance in pregnancy and placental functions such as glycerophospholipid metabolism, polyunsaturated fatty acid metabolism, and steroid hormone biosynthesis. To explore the hypothesis that aspirin delays gestational age advancement and thus the onset of preeclampsia, we constructed a metabolic clock to estimate gestational age in pre-treatment and placebo-treated samples. The results showed that aspirin significantly slowed metabolic gestational ageing by 1.27 weeks (95% confidence interval, 0.66-1.88 weeks) and partially reversed one-fourth of the metabolic changes during gestation.

Conclusion

Aspirin significantly delays the metabolic clock according to estimated gestational age. Aspirin treatment partially reverses a wide range of metabolic changes during gestation. These results strongly support the aspirin-related delay hypothesis.

Funding

This study was supported by the Health and Medical Research Fund, Health Bureau, Hong Kong SAR Government (#06171046). The full report is available from the Health and Medical Research Fund website (https://rfs2.healthbureau.gov.hk). This study was also supported by the Joint Chinese University of Hong Kong-Baylor College of Medicine Center of Medical Genetics, and the Fetal Medicine Foundation (Charity No: 1037116).

Disclosure

The results of this research have been previously published in:

1. Li X, Milosavljevic A, Elsea SH, et al. Effective aspirin treatment of women at risk for preeclampsia delays the metabolic clock of gestation. Hypertension 2021;78:1398-410.

AUTHOR INDEX

Disclaimer

The reports contained in this publication are for reference only and should not be regarded as a substitute for professional advice. The Government shall not be liable for any loss or damage, howsoever caused, arising from any information contained in these reports. The Government shall not be liable for any inaccuracies, incompleteness, omissions, mistakes or errors in these reports, or for any loss or damage arising from information presented herein. The opinions, findings, conclusions and recommendations expressed in this publication are those of the authors of the reports, and do not necessarily reflect the views of the Government. Nothing herein shall affect the copyright and other intellectual property rights in the information and material contained in these reports. All intellectual property rights and any other rights, if any, in relation to the contents of these reports are hereby reserved. The material herein may be reproduced for personal use but may not be reproduced or distributed for commercial purposes or any other exploitation without the prior written consent of the Government. Nothing contained in these reports shall constitute any of the authors of these reports an employer, employee, servant, agent or partner of the Government.

Published by the Hong Kong Academy of Medicine Press for the Government of the Hong Kong Special Administrative Region. The opinions expressed in the *Hong Kong Medical Journal* and its supplements are those of the authors and do not reflect the official policies of the Hong Kong Academy of Medicine, the Hong Kong Medical Association, the institutions to which the authors are affiliated, or those of the publisher.